



UNIVERSITÀ POLITECNICA DELLE MARCHE
Repository ISTITUZIONALE

Energy flexibility curves to characterize the residential space cooling sector: The role of cooling technology and emission system

This is a pre print version of the following article:

Original

Energy flexibility curves to characterize the residential space cooling sector: The role of cooling technology and emission system / Mugnini, A.; Polonara, F.; Arteconi, A.. - In: ENERGY AND BUILDINGS. - ISSN 0378-7788. - 253:(2021). [10.1016/j.enbuild.2021.111335]

Availability:

This version is available at: 11566/295266 since: 2024-11-19T11:50:50Z

Publisher:

Published

DOI:10.1016/j.enbuild.2021.111335

Terms of use:

The terms and conditions for the reuse of this version of the manuscript are specified in the publishing policy. The use of copyrighted works requires the consent of the rights' holder (author or publisher). Works made available under a Creative Commons license or a Publisher's custom-made license can be used according to the terms and conditions contained therein. See editor's website for further information and terms and conditions.

This item was downloaded from IRIS Università Politecnica delle Marche (<https://iris.univpm.it>). When citing, please refer to the published version.

(Article begins on next page)

ENERGY FLEXIBILITY CURVES TO CHARACTERIZE THE RESIDENTIAL SPACE COOLING SECTOR: THE ROLE OF COOLING TECHNOLOGY AND EMISSION SYSTEM

Alice Mugnini^{1*}, Fabio Polonara^{1,2}, Alessia Arteconi^{3,1}

¹Dipartimento di Ingegneria Industriale e Scienze Matematiche, Università Politecnica delle Marche, Via Brecce Bianche 12, 60131, Ancona, Italy

²Istituto per le tecnologie della costruzione, Consiglio Nazionale delle Ricerche, Viale Lombardia 49, 20098, San Giuliano Milanese (MI), Italy

³Department of Mechanical Engineering, KU Leuven, B-3000, Leuven, Belgium

Email: *a.mugnini@univpm.it, f.polonara@univpm.it, a.arteconi@univpm.it

ABSTRACT

Space cooling of buildings shows an increasing trend in energy use worldwide. The exploitation of the energy flexibility reserve obtainable from buildings cooling-loads management can have an important role to improve the security and the reliability of the electricity power grid. Many studies in literature assess the energy flexibility potential of air conditioning systems; however, the role of the specific cooling technology is always scarcely explored. The objective of this work is to provide an evaluation of the operational energy flexibility that can be obtained involving the most common residential space cooling technologies, paying particular attention to the distribution system (e.g., all-air system, fan-coil units with and without the addition of a thermal energy storage and hydronic massive systems). The analysis is carried out with dynamic simulation models for the various cooling systems involved. Results show a great influence of the adopted distribution system in the implementation of a flexibility request. In particular, all-air systems (i.e. split systems) show the lower flexible behavior (they require up to 10 hours of precooling to be off during a peak hour). Whereas the adoption of fan coil units coupled with a thermal energy storage allows to implement different peak shaving strategies without compromising the indoor air temperature with low drawback effects in terms of anticipated electricity overconsumptions (no precooling of the air is required and a maximum of 23 % increase in electricity consumed in the time before the event occurs, with a reduction of 16 % in subsequent hours). In case of ceiling cooling systems, results highlight that as the thermal inertia of the system increases, the indoor conditions are less affected, but the anticipated overconsumption of the heat pump increases (for the same Demand Response event the electricity overconsumption goes from + 67 % to + 116 %, passing from ceiling panels to concrete ceiling). The results obtained from this analysis are then used to draw flexibility curves, which aim at providing a characterization of the flexibility of a cooling system. They can be used to predict, for typical installations, the system behavior in presence of a peak power reduction strategy in terms of pre-cooling duration, energy use variation and modification of the temperature comfort bandwidth. Such predictions are important because they can provide insights on the design and operation of space cooling systems in demand side management strategies.

Keywords: Energy Flexibility, Demand Response, Peak Shaving, Space Cooling, Thermal Distribution System

1. INTRODUCTION

Energy demand for space cooling (SC) has more than tripled worldwide since 1990, making it the fastest-growing end use in buildings [1]. In particular, the residential sector represents the 20 % of the final energy consumption [2]. To enable the use of a large share of renewable energy sources in the electricity generation mix, Demand Side Management (DSM) programs applied to buildings cooling loads can have a paramount role to improve the security of the power grid. DMS is defined as the set of actions aimed at planning, implementing and monitoring of utility activities designed to influence customers' use of electricity [3]. Between them, Demand Response (DR) strategies are considered one of the main solutions to alleviate the issues due to the unpredictability of generation, as they allow the exploitation of the latent flexibility of electrical demand [4]. In particular, a DR event represents a change in electric usage of the end-user from its normal consumption pattern in response to (i) changes in the price of electricity

47 over time, or to (ii) incentive payments designed to induce lower electricity use at times of high wholesale market
48 prices or when system reliability is jeopardized [5].

49 By virtue of the possible presence of different levels of thermal energy storage, buildings contain a relatively large
50 share of demand that can be controlled, adapted and/or enhanced to produce energy flexibility services [6]. Focusing
51 on cooling demand, there are several studies that investigate the potential load-shifting capability of the sector,
52 demonstrating the relevance of this application. Many of them are mainly focused on the evaluation of the energy
53 flexibility performance of the specific case studies analysed. For instance, Li et al. [7] investigated the couple effect
54 of the thermal mass of a commercial building and its air-conditioning system for the realization of DR events.
55 Modelling the dynamic of both the building and the air conditioning system with a white box approach, they obtained
56 an electricity peak reduction of about 17 % with an on-off control and an additional reduction of about 2 % when also
57 the chilled water temperature is controlled. Yan et al. [8] introduced a novel type of multi-timescale cold storage
58 system to activate the energy flexibility of buildings cooling loads. The storage consists of a heat pipe-based natural
59 ice storage subsystem and a dual-operation chiller. They applied the system to a building in Beijing (China) and
60 evaluate an immediate power reduction by 41 % in response to the real-time DR during the peak cooling period on
61 the design day. Arteconi et al. [9] evaluated the benefit of using a Thermal Energy Storage (TES) coupled with heat
62 pumps for the realization of load shifting strategies in cooling season in an industrial building. They evaluated a
63 charging time of 70 hours for the TES if the cold energy produced in the weekends and outside the working hours is
64 used to cool it down. If fully charged, they calculated that the TES could satisfy the building cooling demand for more
65 than one week. Tang et al. [10] demonstrated the capability of the air conditioning system of a commercial building
66 to produce immediate power reductions. They implemented an optimized control logic that foresees the building
67 cooling demand and determines the number and the regulation mode of operating chillers/pumps to be involved during
68 the DR event. With their proposed strategy a 23 % reduction in power can be obtained, maintaining an acceptable
69 zone temperature.

70 Other studies, instead, evaluate the potential load-shifting that can be obtained by the aggregated demand of the air
71 conditioning sector. For example, Malik et. al [11] estimated possible peak load reductions of clusters of residential
72 air-conditioning systems. Using monitored data of a large group of users (808 Australian household dwellings), they
73 evaluated peak demand reductions from 4 to 9 % for the whole New South Wales State when different air-conditioner
74 usage patterns are clustered. Qi et al. [12], introduced a three-stage load decomposition method based on clustering
75 and correlation methodologies to disaggregate the whole-house energy consumption into Air Cooling (AC) loads and
76 baseloads (loads not sensitive to temperature). They considered different usage patterns for the AC systems (a total of
77 19 patterns). Results suggested that the operational DR potential of the AC loads is more reliable and suitable to
78 generate strategies for day ahead scheduling. Huang and Wu [13] presented an analytical method to build an aggregate
79 flexibility model from residential AC systems for building-to-grid integration based on the virtual battery model. The
80 simplified representation of building thermal dynamics in the analytical method is validated with highly reliable
81 models developed in Modelica and Energy Plus. They estimated their analytical method valuable for power system
82 operators to effectively coordinate a large number of flexible building assets with other resources.

83 As demonstrated by the papers cited above, the topic of the energy flexibility obtainable from the management of
84 cooling loads in buildings has received considerable interest from the scientific community. However, the analysis is
85 always focused on the description of a specific application or on the evaluation of the impact of the whole sector,
86 without providing details about the single technologies composing the demand. The role of the particular space cooling
87 technology in the realization of DR events is almost never highlighted. Instead, due to different intrinsic characteristics

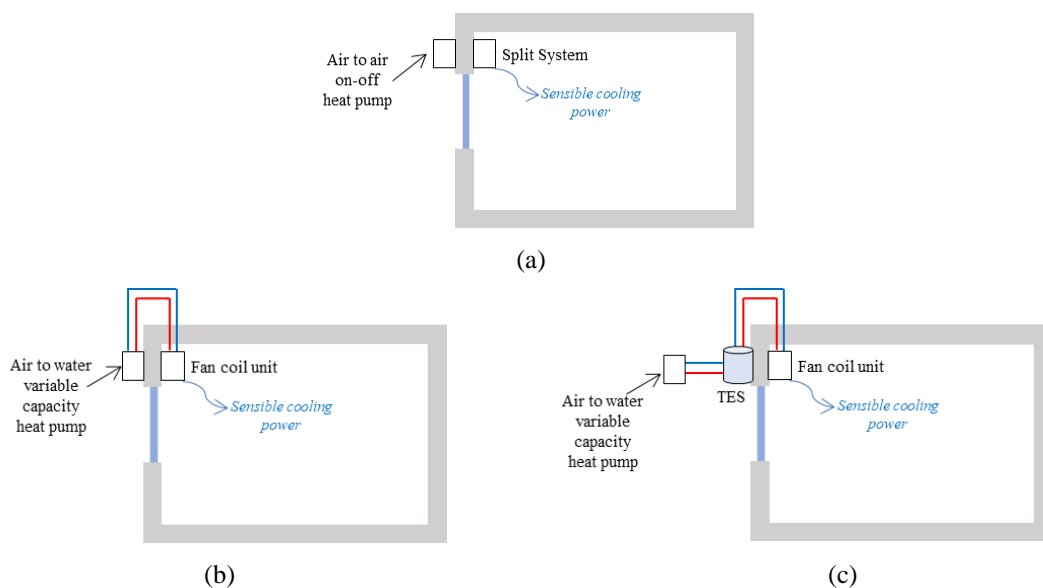
88 that a cooling system can have (e.g., the thermal inertia of the distribution system, the rapidity in demand satisfaction
 89 or the accuracy in the comfort parameters control), it could have a great impact in the way the flexible event is carried
 90 out. Therefore, the objective of this paper is to provide an evaluation of the operative load-shifting capability of the
 91 most common residential space cooling technologies with a focus on the role of the indoor terminal units adopted.
 92 Electric cooling systems are considered (e.g. on-off and variable capacity heat pumps) and three macro-categories of
 93 thermal distribution systems are modelled: all-air systems, fan-coil units and hydronic ceiling cooling systems. In
 94 particular five space cooling technologies are evaluated: split system with on-off regulation, fan coil units with and
 95 without the addition of a sensible TES, ceiling panels with an indoor air dehumidifier and a concrete ceiling cooling
 96 system coupled with an air dehumidifier.
 97 The idea behind this study is to extend the design energy flexibility evaluation [14], already investigated by the authors
 98 in a previous work [15], to the operational scenario by analysing the working conditions of space cooling emission
 99 systems. In addition, flexibility curves for each emission system are proposed as an evaluation tool. These curves
 100 allow to characterize the behaviour of each system in terms of response to different events with an imposed load
 101 variation. They can be considered as an instrument to define guidelines for resources planning and Demand Side
 102 Management strategies. Furthermore, they can provide more technical insights on the specifications of such systems
 103 to support their design as energy flexibility enablers.

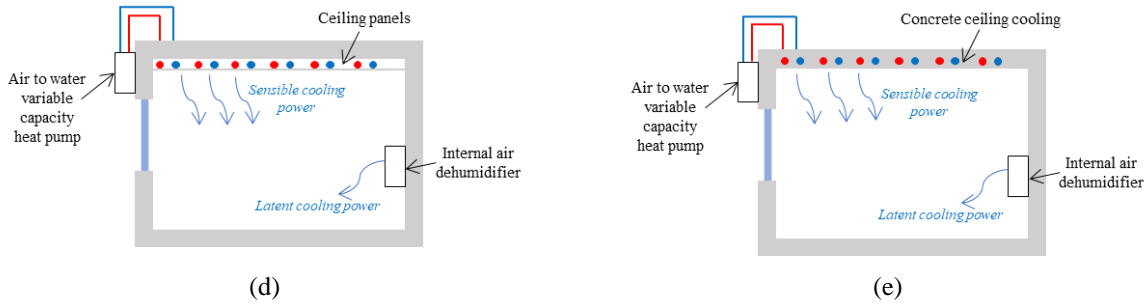
104

105 **2. METHODOLOGY**

106 With the aim of considering all the most widespread technologies at residential level, five different space cooling
 107 systems are modelled (Figure 1): an air to air heat pump with on-off regulation (split system, SS), an air to water heat
 108 pump with fan coil units (FCUs) as distribution system (this configuration is modelled both with and without the
 109 addition of a sensible thermal energy storage, TES) and an air to water heat pump coupled with two different hydronic
 110 ceiling distribution systems (ceiling panels, CP, and concrete ceiling cooling, CC). The latter two differ in their level
 111 of thermal inertia. The first one (CP, Figure 1(d)) is composed of pipes set on panels in the first internal layer of the
 112 roof (medium thermal inertia system) while the cooling concrete ceiling (CC, Figure 1(e)) has high storage capability,
 113 since its pipes are embedded in a high massive concrete layer.

114





115 **Figure 1.** Schematic of the modelled space cooling technologies: (a) split system; (b) variable capacity air to water heat pump with
 116 fan coil unit; (c) variable capacity air to water heat pump with fan coil unit equipped with TES; (d) variable capacity air to water
 117 heat pump with ceiling panels and dehumidifier and (e) variable capacity air to water heat pump with concrete ceiling cooling and
 118 dehumidifier.

119 When split systems and fan coil units are used, only the internal temperature can be directly controlled as comfort
 120 condition (with an indirect control over humidity through low supply temperature) while, in case of ceiling systems
 121 (CC and CP), a relative humidity punctual control must also be provided in order to guarantee a comfortable
 122 environment. Therefore, for these cases, the treatment of latent heat is entrusted to an internal air dehumidifier (DH).
 123 Table 1 reports the five considered cooling systems with a description of their main characteristics in terms of comfort
 124 parameters control, rapidity of satisfying the thermal demand and energy storage capacity.

125 **Table 1.** Space cooling technologies modelled and their main characteristics.

SC characteristics	SS	FCU	FCU with TES	CP	CC
Generation system	Air to air HP with on-off regulation	Air to water variable capacity HP	Air to water variable capacity HP	Air to water variable capacity HP and dehumidifier	Air to water variable capacity HP and dehumidifier
Distribution system	Internal unit of split system	Fan coil units (low supply temperature)	Fan coil units with TES (low supply temperature)	Ceiling panels (high supply temperature)	Concrete ceiling cooling (high supply temperature)
Comfort parameters controlled	Temperature	Temperature	Temperature	Temperature and humidity	Temperature and humidity
Rapidity of demand satisfaction	High	High	High	Medium	Low
Storage capability	Absent	Absent	From low to high in relation to the TES size	Medium-low	High

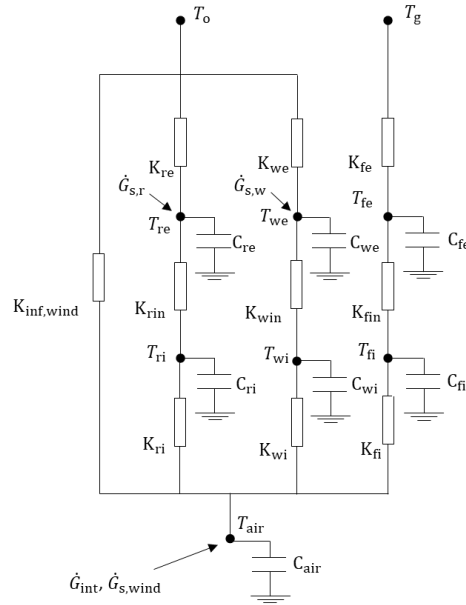
126 The description of the modeling approach adopted to obtain the dynamic behavior of each cooling system is reported
 127 in Section 2.1, where details about the building model are included. A building with the same thermal and geometrical
 128 properties is considered for all the space cooling systems, thus alleviating the influence of the building characteristics
 129 on the comparison analysis. Then, in Section 2.2, the Demand Response events are described and details about their
 130 formulation and implementation are provided. Finally, in Section 2.3, some parameters to evaluate the operational
 131 flexibility are introduced: they are adopted to build the flexibility curves in order to provide an instrument to easily
 132 compare the performance of the different cooling systems under different points of views.
 133

135 2.1 Thermal model of the space cooling systems

136 In order to model the building thermal dynamics, a detailed (10 thermal resistances and 7 thermal capacitances)
 137 lumped-parameter model based on the thermal-electricity analogy is used [16]. A common structure is used for all the
 138 space cooling technologies (Figure 2). The parameters of the network of thermal resistances and capacitances (RC-

139 network) are identified with a white box approach according to the thermal and geometrical characteristics of a
 140 reference building. In Figure 2 is represented the thermal conductance (K), defined as the reciprocal of thermal
 141 resistance.

142 To represent the short-term dynamic of a building with good performance accuracy and low computational cost, each
 143 opaque surface of the building envelope is modelled with two capacitances (thermal nodes) and three thermal
 144 resistances according with the model architecture proposed by Boodi et al. [17]. In particular, the two thermal
 145 capacities represent all the layers of the surface in the positions preceding and following the thermal insulation.
 146 Consequently, the two temperatures are the surface temperatures of the insulation layer. The numerical values of
 147 thermal resistances (R) and capacitances (C) are calculated taking inspiration from the approach proposed in EN ISO
 148 13790 standard [18] (developed for a simple 5R1C building model). The numerical values of the parameters are
 149 reported in Section 3 where the case study is described.



150
 151 **Figure 2.** 10R7C network building model.

152 Assuming one-dimensional heat transfer, the system dynamics can be described as a classic linear state-space model:

$$d\mathbf{X}(t) = \mathbf{A} \cdot \mathbf{X}(t)dt + \mathbf{B} \cdot \mathbf{U}(t)dt \quad \text{Eq. 1}$$

$$\mathbf{Y}(t) = \mathbf{C} \cdot \mathbf{X}(t)dt + \mathbf{D} \cdot \mathbf{U}(t)dt \quad \text{Eq. 2}$$

153 where $\mathbf{X}(t)$ is the state-space vector, $\mathbf{U}(t)$ is the input vector and $\mathbf{Y}(t)$ represents the output vector. \mathbf{A} , \mathbf{B} , \mathbf{C} and \mathbf{D} are
 154 time-invariant real matrices depending on the parameters of the network.

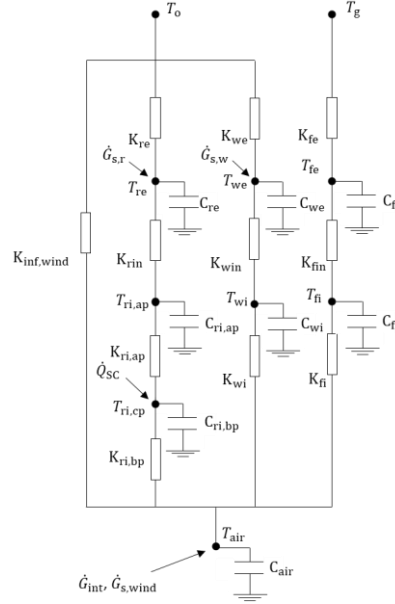
155 As can be noted in Figure 2, the contribution of the cooling system (\dot{Q}_{SC}) is not shown, since the way it is supplied
 156 depends on the specific space cooling technology. Indeed, when the cooling system is composed of an air distribution
 157 system (e.g. split systems and fan coil units), \dot{Q}_{SC} is directly removed from the internal air node temperature (T_{air}).
 158 Instead, in case of addition of a thermal energy storage to the fan coil water circuit, the thermal power that is supplied
 159 to the internal air thermal node ($\dot{Q}_{building}$) is decoupled from that produced by the cooling system (\dot{Q}_{SC}). Their link is
 160 formalized in the thermal energy storage (TES) model (Equation 3) [19]:

$$C_{TES} \cdot \frac{dT_{TES}}{dt} = \dot{Q}_{SC} + \dot{Q}_{building} + L_{TES}(T_{env} - T_{TES}) \quad \text{Eq. 3}$$

161 The TES is assumed to be a perfectly mixed water tank. Its storage capability is modelled with a thermal capacitance
 162 (C_{TES}) and with a temperature node (T_{TES}). The thermal losses with the environment temperature (T_{env}) are modelled

163 with a loss coefficient factor (L_{TES}). Although Equation 3 introduces an approximation in the modeling of the tank
 164 (i.e. the stratification is neglected) this is considered acceptable for the purposes of the analysis proposed in this work
 165 since, dealing with the summer case, the temperature difference granted to the tank is quite small (5 ° C as will be
 166 seen in Section 3).

167 In case of ceiling cooling systems (ceiling panels, CP, and concrete ceiling cooling, CC), \dot{Q}_{SC} is removed from the
 168 inner roof thermal node. In case of high massive system (CC) this node coincides with the node T_{ri} in Figure 2, while
 169 for the ceiling panels (CP) a further thermal node for the ceiling is distinguished ($T_{ri,cp}$, which stands for the position
 170 immediately after the internal plaster, in Figure 3).



171
 172 **Figure 3.** 11R8C network for CP system sensible model.

173 In these last two space cooling systems (CC and CP), also the humidity control is enabled. With reference to the
 174 effective capacitance humidity model [20], the moisture balance is carried out in parallel with the sensible energy
 175 balance calculation. For the air node it is expressed as:

$$M_{air} \frac{dx_{air}}{dt} = \dot{m}_{vent}(x_o - x_{air}) + \frac{\dot{Q}_{DH}}{h_v} \quad \text{Eq. 4}$$

176 Where M_{air} and x_{air} are the mass and the absolute humidity of the internal air, \dot{m}_{vent} and x_o are the natural ventilation
 177 flowrates and its absolute humidity, \dot{Q}_{DH} is the latent contribution of the dehumidifier systems and h_v is the heat of
 178 evaporation of water (approximately assumed constant in the balance).

179
 180 **2.2 Demand Response event**

181 The capability of a space cooling system to respond to a programmed load variation is evaluated by simulating
 182 different Demand Response events and comparing them with a reference case (Baseline). The Baseline (BL) is
 183 represented by the demand curve of each cooling system able to maintain the comfort conditions. It is computed as
 184 the solution of a linear optimization problem that has the objective of minimizing the thermal requirement of the
 185 building:

$$\text{minimize} \left(\sum_{k_{start}}^{k_{end}} \dot{Q}_{SC}(k) \cdot \Delta k \right) \quad \text{Eq. 5}$$

186 where k is the discrete time and Δk the simulation timestep, which has been set equal to 0.1 hours (6 minutes).
 187 Here, the thermal power of the cooling system (\dot{Q}_{SC}) is the decision variable of the optimization problem and it is
 188 limited at each timestep (Δk) by the maximum power of the generating system. A distinction has to be made between
 189 the optimization problem solved for the split system (i.e., on/off regulation) and the other cooling systems (i.e., FCU,
 190 CP and CC). Actually, if for the FCU, CP and CC systems a typical linear programming optimization problem is
 191 written (Equation 5), for the split a MILP (mixed-integer linear programming) is introduced to reproduce the on-off
 192 regulation. In this case, the optimization problem is represented in Equation 5 as:

$$\text{minimize} \left(\sum_{k_{\text{start}}}^{k_{\text{end}}} \dot{Q}_{\text{full-load}}(k) \cdot CTRL_{SS}(k) \cdot \Delta k \right) \quad \text{Eq. 6}$$

193 where $CTRL_{SS}$ is the Boolean decision variable for the split system and it is limited at each timestep by the maximum
 194 power of the generating system ($\dot{Q}_{\text{full-load}}$).

195 The comfort constraints on the air temperature node must be satisfied. They are modelled with a setpoint temperature
 196 (T_{sp}) and an allowed comfort band defined with a $\Delta T_{sp,max}$ (upper comfort band) and a $\Delta T_{sp,min}$ (lower comfort band):

$$\forall k \quad (T_{sp} - \Delta T_{sp,min}(k)) \leq T_{air}(k) \leq (T_{sp} + \Delta T_{sp,max}(k)) \quad \text{Eq. 7}$$

197 Moreover, if the cooling system is able to control also the internal humidity, the same condition expressed in Equation
 198 7, can be written for the relative humidity (RH):

$$\forall k \quad (RH_{sp} - \Delta RH_{sp,min}(k)) \leq RH(k) \leq (RH_{sp} + \Delta RH_{sp,max}(k)) \quad \text{Eq. 8}$$

199 The constraint formulated in Equation 8, is actually mathematically expressed in terms of absolute humidity (x).
 200 Therefore, the effective constraint is:

$$\forall k \quad x_{\min}(k) \leq x_{air}(k) \leq x_{\max}(k) \quad \text{Eq. 9}$$

201 With x_{\min} and x_{\max} calculated as the absolute humidity at the allowed upper comfort limit for the temperature
 202 ($T_{sp} + \Delta T_{sp,max}$) and respectively the lower ($RH_{sp} - \Delta RH_{sp,min}$) and the upper ($RH_{sp} + \Delta RH_{sp,max}$) comfort limit
 203 for the relative humidity.

204 When the cooling power is not directly provided to the internal air node (T_{air}) (e.g., for fan coil units coupled with
 205 TES, ceiling panels or cooling concrete ceiling systems), a constraint on the temperature of the thermal mass (TMD)
 206 of the distribution system node is required:

$$\forall k \quad T_{TMD,min} \leq T_{TMD}(k) \leq T_{TMD,max} \quad \text{Eq. 10}$$

207 In particular, T_{TMD} coincides with T_{TES} for the cooling system composed of fan coil units and TES, $T_{ri,cp}$ for ceiling
 208 panels and T_{ri} for concrete ceiling cooling system.

209 The Demand Response event is a peak shaving strategy (PSS). It is modeled by imposing at a certain time $k_{\text{start,DR}}$
 210 and for a period Δk_{DR} a variation of the electrical power peak of the Baseline, according to a reduction factor (f_{PSS}).

$$\text{For } k_{\text{start,DR}} \leq k \leq k_{\text{end,DR}} \quad \dot{P}_{DR} = f_{PSS} \cdot \dot{P}_{\text{max,BL}} \quad \text{Eq. 11}$$

211 With: $k_{\text{end,DR}} = k_{\text{start,DR}} + \Delta k_{DR}$

212 This condition is modelled as an additional constraint for the optimization problem:

$$\forall k \quad \dot{P}_{SC}(k) \leq \dot{P}_{DR}(k) \quad \text{Eq. 12}$$

213 where \dot{P}_{SC} is the electrical absorption of the individual cooling systems. The condition imposed by Equation 12 is
 214 converted in terms of a constraint on the thermal power, by means of the knowledge of the heat pump performance
 215 function (EER), which depends on the external temperature, supply temperature and capacity ratio and that is known
 216 at the time of the DR event.

245 (i) The use of the energy flexibility of the thermal mass of the distribution system (TMD). This quantity can be
 246 calculated only in cases in where the cooling power produced by the generation system is removed to a
 247 thermal node (T_{TMD}) different from the internal air node (T_{air}): therefore in case of FCU with the addition of
 248 the TES (T_{TMD} coincides with T_{TES}), CC (T_{TMD} coincides with T_{ri}) and CP (T_{TMD} coincides with $T_{ri,cp}$).
 249 The strategy that can be implemented is the pre-cooling of this thermal mass in the hours preceding the event.
 250 To estimate this exploitation, the quantity $Flex_{TMD}$ (in percentage) is calculated. It represents the variation
 251 between the Demand Response and the Baseline scenario of the temperature of the distribution system
 252 thermal mass (T_{TMD}), referred to the Baseline:

$$Flex_{TMD} = \frac{T_{TMD,DR} - T_{TMD,BL}}{T_{TMD,BL}} \quad \text{Eq. 13}$$

253 (ii) The use of the energy flexibility of thermostatically controlled loads (TCLs). Again, the strategies that can
 254 be implemented are the pre-cooling of the internal air in the hours preceding the event and the raising of the
 255 temperature during the event (Δk_{DR}). To estimate this exploitation, the quantity $Flex_{TCL}$ (in percentage) is
 256 calculated. It represents the variation between the Demand Response and the Baseline scenario of the
 257 temperature of the internal air thermal node (T_{air}), referred to the air temperature of the Baseline:

$$Flex_{TCL} = \frac{T_{air,DR} - T_{air,BL}}{T_{air,BL}} \quad \text{Eq. 14}$$

258 If a humidity control is possible for the cooling system, the same quantity can be calculated for the relative
 259 humidity (RH):

$$Flex_{RH} = \frac{RH_{DR} - RH_{BL}}{RH_{BL}} \quad \text{Eq. 15}$$

260 Furthermore, the pre-cooling time interval (Δk_{prec}) is calculated as the time period (before the DR event) in
 261 which the air temperature in Demand Response scenario is lower than in the Baseline.

262 (iii) The payback load in the electricity power curve. This effect can derive both from the use of the flexibility
 263 from thermostatically controlled loads and from the exploitation of the thermal inertia of the system. It is
 264 represented both by the electric power variation \dot{P}_{shift}^* (\dot{P}_{rated} represents the rated electricity power of the
 265 specific space cooling technology):

$$\dot{P}_{shift}^* = \frac{\dot{P}_{DR} - \dot{P}_{BL}}{\dot{P}_{rated}} \quad \text{Eq. 16}$$

266 and also by the energy consumption variation (in percentage terms) in the time before and after the Demand
 267 Response event:

$$E_{shift,bDR} = \frac{\sum_{k=k_{strat}}^{k_{strat,DR}} (\dot{P}_{DR}(k) - \dot{P}_{BL}(k)) \Delta k}{\sum_{k=k_{strat}}^{k_{strat,DR}} \dot{P}_{BL}(k) \Delta k} \quad \text{Eq. 17}$$

$$E_{shift,aDR} = \frac{\sum_{k=k_{end,DR}}^{k_{end}} (\dot{P}_{DR}(k) - \dot{P}_{BL}(k)) \Delta k}{\sum_{k=k_{end,DR}}^{k_{end}} \dot{P}_{BL}(k) \Delta k} \quad \text{Eq. 18}$$

268 As it can be noted, the quantities introduced make it possible to evaluate which source of flexibility is exploited by
 269 the plant (i.e. TMD or TCLs) and to what extent this occurs. Thanks to the quantities presented, two levels of analysis
 270 are possible.

- 271 • The first allows to timely and punctually evaluate the behavior of the plant during the Demand Response event
 272 with reference to the baseline. Indeed, with $Flex_{TMD}$, $Flex_{TCL}$, $Flex_{RH}$ it is possible to appreciate the extent of

273 activation of the various sources of flexibility and thanks to \dot{P}_{shift}^* their feedback on the temporal variation of the
 274 electric power can be assessed.

- 275 • On the other side, with the calculation of the parameters: Δk_{prec} (duration of the pre-cooling of the internal air),
 276 $E_{\text{shift,bDR}}$ and $E_{\text{shift,aDR}}$ (i.e. energy consumption variation in the time before and after the event), it is possible to
 277 summarize the impact on the user setpoint and on electricity demand.

278 It is precisely from the calculation of these two parameters under different Demand Response events (i.e. peak
 279 reduction amount) that the flexibility curves can be obtained. Therefore, the flexibility curves have the objective of
 280 characterizing the behavior of an emission system and they represent an instrument to quickly predict the response of
 281 the system.

282

283 3. DYNAMIC MODEL

284 A dynamic model to analyze the behavior of the different cooling systems has been developed. The latter are supposed
 285 installed in a typical Italian building, representative of the building stock. This choice helps to obtain results that can
 286 be easily generalized. The thermal characteristics of the building are extrapolated by Tabula Project [22]. In particular,
 287 a single-family house is selected with construction period after 2006. The value of the thermal transmittances of the
 288 single opaque and transparent surfaces are reported in Table 2. The stratigraphy and the materials composing the
 289 individual parts of the building envelope are chosen with reference to [23]. Hourly air changes of 0.2 h^{-1} are used and
 290 the internal gains (due to occupation and equipment) are evaluated with [18]. To obtain the environmental conditions
 291 (outdoor temperature and solar radiation), a climate file is adopted (Rome $41^\circ 53' \text{ N } 12^\circ 28' \text{ E}$) [24].

292 **Table 2.** Thermal transmittances (U-value) for the single opaque and transparent surfaces of the building.

External walls ($\text{W m}^{-2}\text{K}^{-1}$)	Roof ($\text{W m}^{-2}\text{K}^{-1}$)	Floor ($\text{W m}^{-2}\text{K}^{-1}$)	Windows ($\text{W m}^{-2}\text{K}^{-1}$)
0.34	0.28	0.33	2.20

293

294 In case of presence of a thermal energy storage in the fan coil water circuit, a typical storage system suitable for heat
 295 pumps [25] of 750 liters (0.75 m^3) is introduced. Considering the Vitocell 100-E series (type SVP/SVPA), the catalog
 296 reports an internal diameter (without insulation) of 0.79 m and a thermal coefficient loss per area of $0.68 \text{ W m}^{-2} \text{ K}^{-1}$.
 297 Since it is used for cooling its internal temperature (T_{TES}) will be in the range $7\text{-}12 \text{ }^\circ\text{C}$ (Equation 10). According to
 298 the same logic, also the temperature of the nodes from which heat is removed in the ceiling panels and in the cooling
 299 concrete ceiling systems ($T_{\text{ri,cp}}$ and T_{ri}) are limited in the interval $18\text{-}26 \text{ }^\circ\text{C}$ to avoid thermal discomfort.

300 Table 3 shows all the RC-network parameters values obtained for the case study.

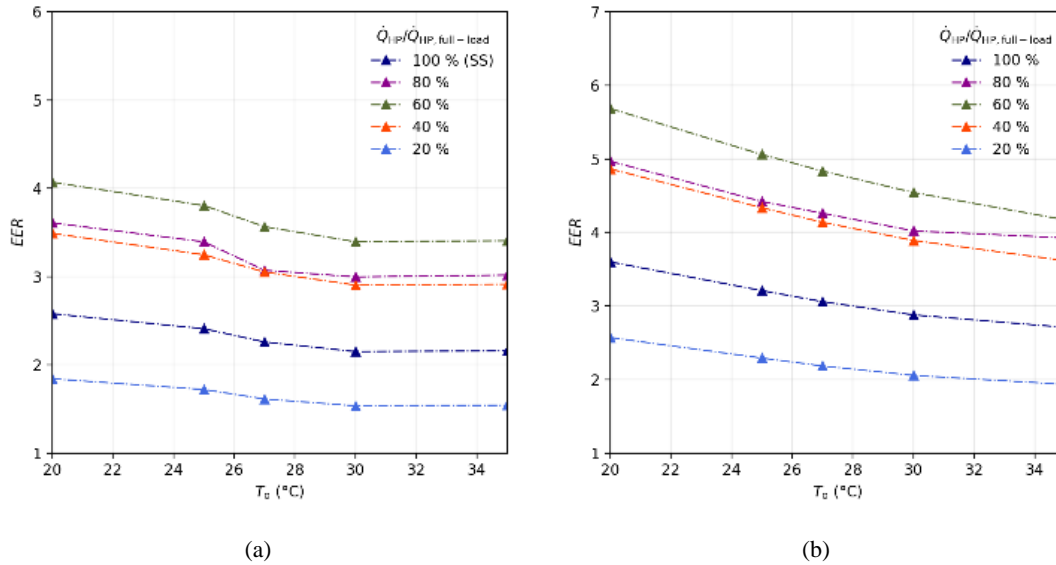
301

Table 3. Numerical value of parameters.

Thermal conductance (W K^{-1})	Thermal capacity (kWh K^{-1})
$K_{\text{inf,wind}}$	C_{we}
K_{we}	C_{wi}
K_{win}	C_{re}
K_{wi}	C_{ri}
K_{re}	$C_{\text{ri,ap}}$
K_{rin}	$C_{\text{ri,bp}}$
K_{ri}	C_{fe}
$K_{\text{ri,ap}}$	C_{fi}
$K_{\text{ri,bp}}$	C_{air}
K_{fe}	C_{TES}
K_{fin}	
K_{fin}	
K_{l}	

302

303 To model the cooling generation systems, a commercial variable capacity heat pump (HP) is selected (Vitocal
 304 B04/A04) [26]. It is an air to water heat pump of 3.8 kW_{th} and *EER* of 2.16 with a water supply temperature of 7 °C
 305 and an outdoor temperature of 35 °C (performances become 4.7 kW_{th} and *EER* of 2.71 with a water supply temperature
 306 of 18 °C and an outdoor temperature of 35 °C). For the on-off air-to-air heat pump, the full load performances of [26]
 307 with a flow temperature of 7 °C. For the fan coil model, the performances are evaluated with a supply temperature of
 308 7 °C while for the ceiling distribution systems (CC and CP) it is fixed to 18 °C. Figure 5 shows the COP trend of the
 309 modelled heat pumps by varying the ambient temperature and the thermal capacity.
 310



311 **Figure 5.** Performance (*EER*) of the heat pumps by varying the outside temperature (*T_o*): (a) variable capacity heat pump for a
 312 fixed water supply temperature of 7 °C and (b) variable capacity heat pump for a fixed water supply temperature of 18 °C.

313 As mentioned, for the hydronic radiant cooling systems (CC and CP), it is possible to control also the humidity, by
 314 using an air dehumidifier (DH). Its characteristics are selected with references to commercial DH to be combined with
 315 ceiling systems [27]. In particular, the IN+ 300 model is chosen. It has a dehumidification capacity of 20.8 l day⁻¹ with
 316 an electricity absorption of 320 W_e.

317 In Table 4 are summarized all the parameters used to simulate the space cooling technologies.

318 **Table 4.** Parameters used to simulate the cooling systems.

SS		FCU		CP and CC	
Heat pump		Heat pump		Heat pump	
Design supply temperature	7 °C	Design supply temperature	7 °C	Design supply temperature	18 °C
Thermal power (W7A35)	3.8 kW _{th}	Thermal power (W7A35)	3.8 kW _{th}	Thermal power (W18A35)	4.7 kW _{th}
COP (W7A35)	2.16	COP (W7A35)	2.16	COP (W18A35)	2.71
Regulation	On-off	Regulation	Power regulation from 30 % of maximum load	Regulation	Power regulation from 30 % of maximum load
TMD		TMD		TMD	
Location	Absent	Location	Available in case of TES addition	Location	Roof layer
		Constraints	7-12 °C	Constraints	18-26 °C
		Volume	75 liters		
DH		DH		DH	
Absent		Absent		Capacity	20.8 liters day ⁻¹
				Electricity absorption	320 W _e

319

320 4. RESULTS

321 A summer representative day is selected to analyze the systems operation. It is selected as the day in which the average
322 daily outdoor air temperature is closer to the daily monthly average outdoor air temperature of the wheatear data (5
323 July). By varying the day on which the event occurs, slightly different values are obtained, without affecting the
324 overall conclusions. Thus the general considerations on the flexibility curves for the different emission systems remain
325 valid regardless of the chosen day.

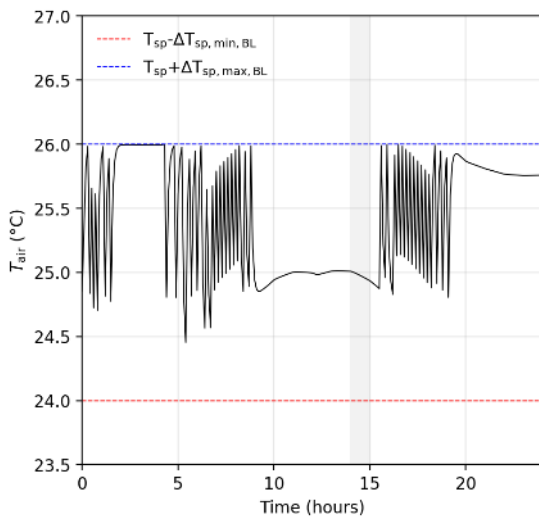
326 In the next paragraph (Section 4.1), the characteristics of the individual Space Cooling technologies in Demand
327 Response scenarios will be described in relation to the relative Baseline; both the dynamic behavior and the flexibility
328 curves are discussed. Then, in Section 4.2, a comparison between the various systems is provided.

329 4.1 Assessment of operational flexibility for the single Space Cooling technologies

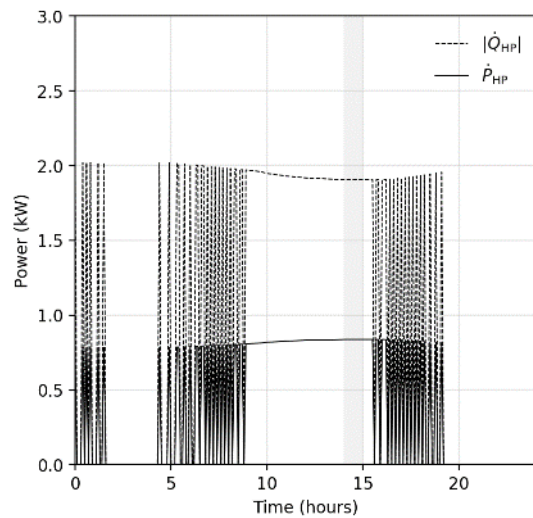
331 In order to assess the punctual behavior of the single technology in a load-shifting scenario, the dynamic behavior of
332 each cooling system is described firstly with reference to the same peak shaving event, and then under different
333 conditions. In order to obtain a characterization as complete as possible of the load-shifting capability of the systems,
334 the parameters that characterize the DR event (f_{PSS} , $\Delta T_{sp,max,DR}$, $\Delta T_{sp,min,DR}$, $\Delta RH_{sp,max,DR}$ and $\Delta RH_{sp,min,DR}$) are varied in
335 the analysis. For simplicity, only Demand Response events that start at the peak time are considered ($k_{start,DR}$ equal to
336 $k_{peak,BL}$). Moreover, although not very applicable in practice, except for more modern thermostats, variations in very
337 narrow boundary conditions (i.e., 0.1 °C) for the setpoints ($\Delta T_{sp,max,DR}$ and $\Delta T_{sp,min,DR}$) are also tested in order to map
338 the behavior of the individual systems.

339 4.1.1 Split System (SS) with on-off operation

341 When the cooling demand of the building is satisfied with an on-off split system (SS), the temperature of the air node
342 (T_{air}) cannot be maintained at the constant value of the setpoint (T_{sp} of 26 °C) but it oscillates within the band allowed
343 by the thermostat (Figure 6(a)). As can be seen from Figure 6(a), due to the intermittent operation of the heat pump it
344 was necessary to set a rather high low tolerance to the setpoint ($\Delta T_{sp,min,BL}$ of 2 °C) throughout the day also in case of
345 BL. In Figure 6(b) the thermal and electric power consumption of the heat pump in case of Baseline operation is
346 shown. In particular, the daily cooling energy demand is 21.8 kWh_{th}, while the electricity consumption is 9.2 kWh_e.
347 The electricity peak power is 0.84 kW_e and occurs at 2.00 pm.



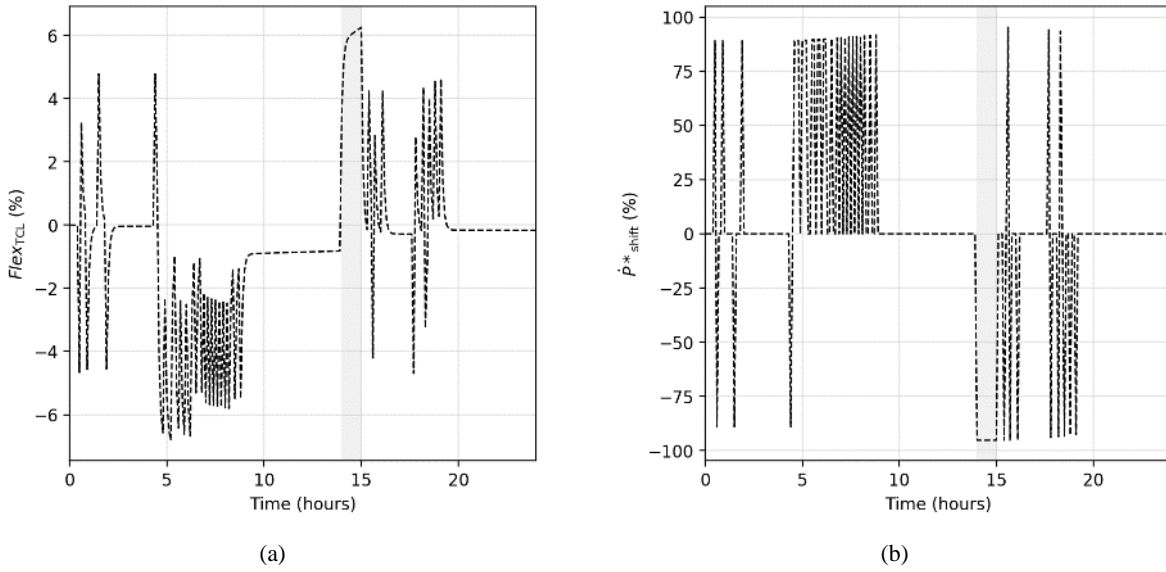
(a)



(b)

348 **Figure 6.** Daily Baseline operation for SS with on-off regulation: (a) internal air node temperature and (b) thermal and electrical
 349 HP power.
 350

351 Since no modulation of the heat pump can be exploited, only a Demand Response event with a reduction factor (f_{PSS})
 352 equal to zero can be tested. It is not possible the realization of Demand Response events located at the peak ($k_{start,DR}$
 353 equal to $k_{peak,BL}$) and lasting longer than a timestep (6 minutes) with $\Delta T_{sp,max,DR}$ equal to 0 °C. Accordingly, a certain
 354 upper comfort limit must be guaranteed during the event (i.e. $\Delta T_{sp,max,DR}$ different from 0 °C). In Figure 7 the behavior
 355 of the split system in term of the use of the energy flexibility of thermostatically controlled loads (Figure 7(a)) is
 356 represented, and the presence of payback loads in the electricity power curve (Figure 7(b)) when an event of 1 hour is
 357 tested with an upper comfort band ($\Delta T_{sp,max,DR}$) of 0.5 °C as well. As can be seen, the implementation of the event
 358 requires a large activation of the energy flexibility from TCLs. Indeed, the calculated pre-cooling time interval (Δk_{prec})
 359 is about 10.2 hours and for all the duration of the event (area highlighted in gray in Figure 7(a)) all the upper comfort
 360 band ($\Delta T_{sp,max,DR}$) is exploited. Given the cycling of the system, it is difficult to compare the power trend in the Baseline
 361 and in the Demand Response scenario, therefore it is not possible to distinguish graphically the exact occurrence of
 362 payback loads (Figure 7(b)). Therefore, the planning of a strategy by a potential supervisor (aggregator) would appear
 363 rather complicated given the difficulty in predicting rapid sequences of on and off cycles in the period preceding the
 364 event. However, in the case showed in Figure 7, a + 28.7 % of $E_{shift,bDR}$ is calculated considering the time before the
 365 event, while a $E_{shift,aDR}$ of - 7.8 % is obtained considering the electricity variation after the DR event.

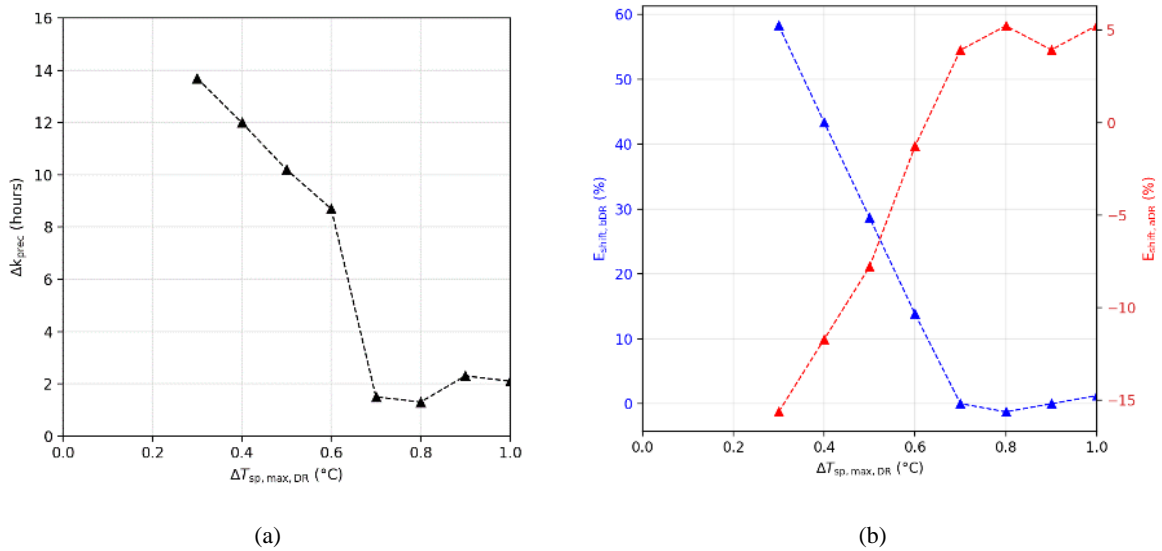


366 **Figure 7.** Daily Demand Response operation (f_{PSS} equal to 0, Δk_{DR} of 1 hour, $\Delta T_{sp,min,DR}$ of 2 °C, $\Delta T_{sp,max,DR}$ of 0.5 °C and $k_{start,DR}$
 367 coinciding with $k_{peak,BL}$) for SS with on-off regulation: (a) $Flex_{TCL}$ and (b) \dot{P}^*_{shift} .
 368

369 Since, as mentioned, only Demand Response events with reduction factor (f_{PSS}) equal to 0 can be realized, the
 370 parameters that can be varied are the lower and the upper comfort bands (i.e. $\Delta T_{sp,min,DR}$ and $\Delta T_{sp,max,DR}$). Moreover,
 371 not all the thermostat variations allow to find a feasible solution for the optimization problem and therefore to realize
 372 the peak shaving event. Figure 8 reports the flexibility curves obtained for the split system. As can be noted, they are
 373 referred to a fixed value of lower comfort band ($\Delta T_{sp,min,DR}$ equal to 2 °C) as lower values are not feasible in the
 374 optimization problem (the split system appears rather inflexible in producing load variations).

375 By activating the energy flexibility from TCLs, the peak cannot be zero with an upper comfort band ($\Delta T_{sp,max,DR}$) lower
 376 than 0.3 °C. On the contrary, allowing higher upper comfort bands, the event can be realized with rather short times
 377 of pre-cooling of the air temperature (up to 0.6 °C for the $\Delta T_{sp,max,DR}$ the precooling is higher than 8.7 hours, while for

378 higher values of $\Delta T_{sp,max,DR}$ the pre-cooling is always lower than 2.25 hours). Anyhow, given the limited number of
 379 possible cases for this type of cooling system, flexibility curves represent only the behavior in a few points (Figure
 380 8).



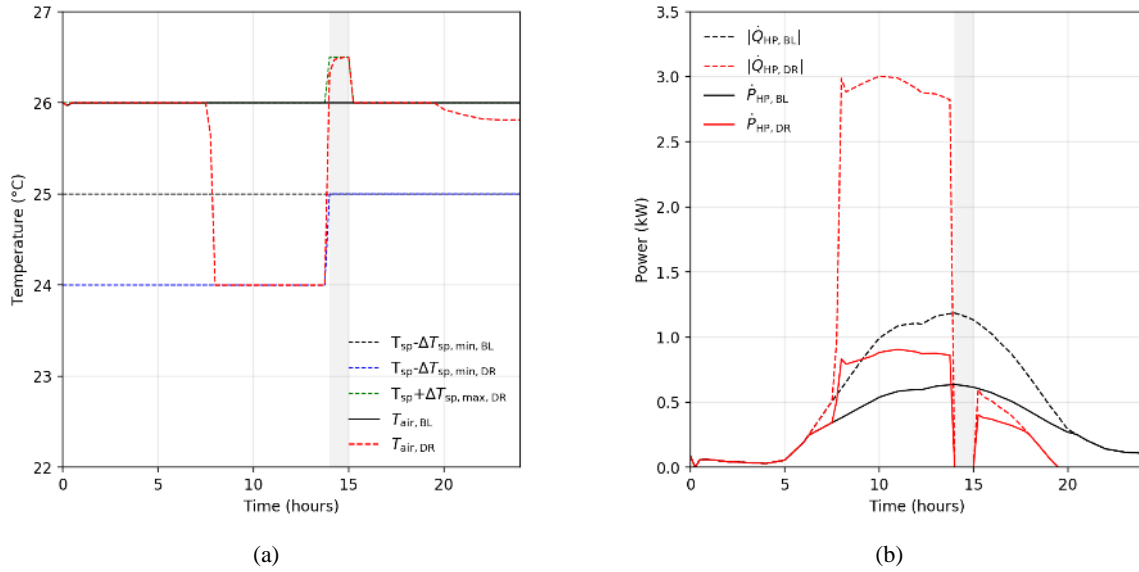
381 **Figure 8.** Flexibility curves for split system with on-off regulation (f_{PSS} equal to 0, Δk_{DR} of 1 hour and $\Delta T_{sp,min,DR}$ equal to 2 °C):
 382 (a) Pre-cooling of the internal air node duration (Δk_{prec}) and (b) $E_{shift,bDR}$ and $E_{shift,aDR}$.

383

384 4.1.2 Fan coil Units (FCUs)

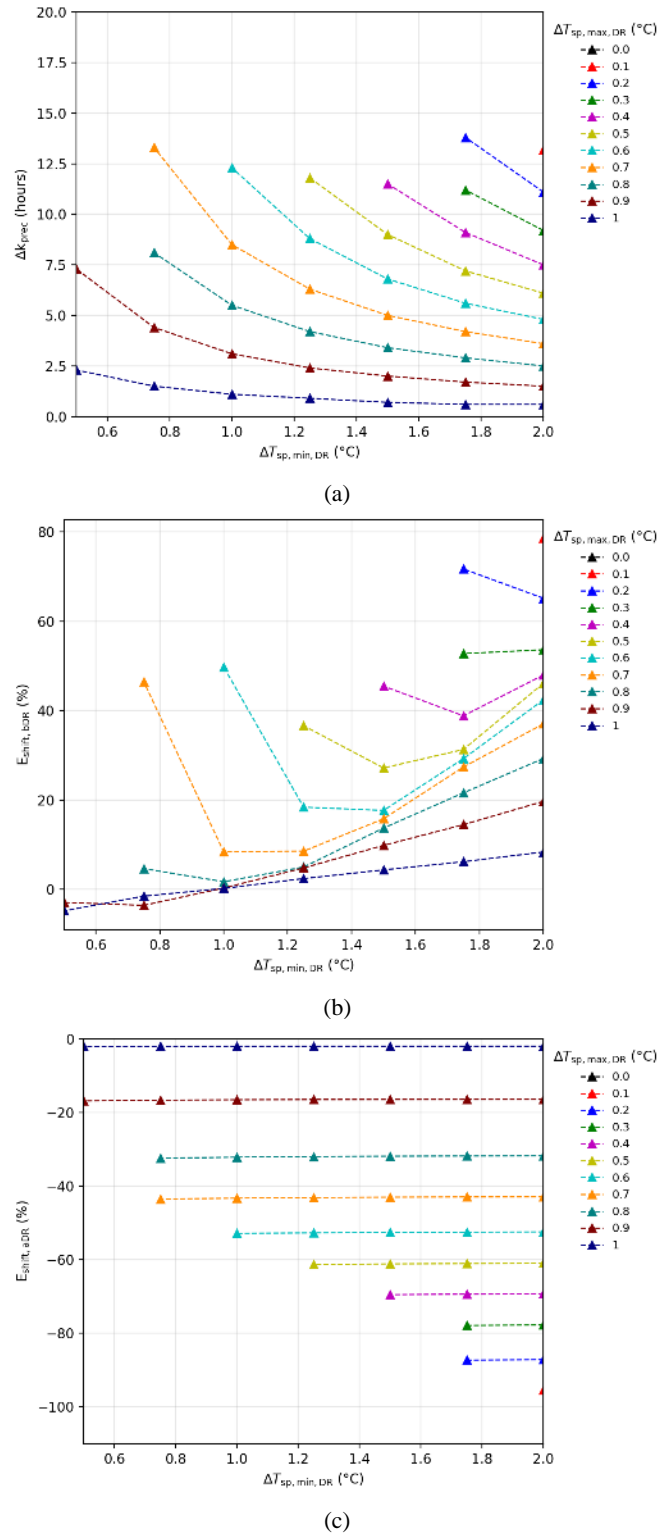
385 If a variable capacity heat pump coupled with fan coil units is used to cover the cooling demand of the building,
 386 different electricity peak reductions can be obtained allowing a certain margin of flexibility to the indoor air
 387 temperature (T_{air}). In Figure 9(a) the same peak shaving event tested for the split system (Figure 7), in which a
 388 cancellation of the electricity peak (f_{PSS} equal to 0) is imposed for 1 hour (Δk_{DR} of 1 hour), is shown in comparison
 389 with the Baseline. In this case, the electricity peak is about 0.64 kW_{el} and it occurs at 2.00 pm. The flexibility range
 390 allows a lower band ($\Delta T_{sp,min,DR}$) of 2 °C and an upper band ($\Delta T_{sp,max,DR}$) of 0.5 °C.

391 In absence of thermal inertia, the flexibility provided by TCLs is exploited by means of a pre-cooling of about 6.25
 392 hours and of a temperature rising (of 0.5 °C) during the event. Clearly, the extent of such flexibility exploitation
 393 depends on the possible temperature setpoints limits granted. However, due to the availability of such a single source
 394 of flexibility, not all the peak reductions can be realized (i.e., the optimization problem finds a feasible solution) and
 395 a great involvement of the temperature setpoints variation is generally required.



396 **Figure 9.** Daily comparison between BL and DR event (f_{PSS} equal to 0, Δk_{DR} of 1 hour, $\Delta T_{sp, min, DR}$ of 2 °C, $\Delta T_{sp, max, DR}$ of 0.5 °C
 397 and $k_{start, DR}$ coinciding with $k_{peak, BL}$) for FCU without TES: (a) internal air node temperature and (b) thermal and electrical power
 398 of the heat pump.
 399

400 In Figure 10 the flexibility curves to produce a 100 % reduction of the electricity consumption in 1 hour (Δk_{DR})
 401 according to the different values of the upper and lower comfort bands (i.e. $\Delta T_{sp, max, DR}$ and $\Delta T_{sp, min, DR}$) are presented.
 402 It can be noticed that as the upper comfort band decreases, it also decreases the number of configurations in which the
 403 peak shaving can be realized. The results reported in Figure 10(a) highlight the role of the two comfort bands values
 404 ($\Delta T_{sp, max, DR}$ and $\Delta T_{sp, min, DR}$). In particular, if the upper comfort band assumes values between 0.9 °C and 1 °C, the event
 405 (f_{PSS} equal to 0 and Δk_{DR} of 1 hour) can be realized regardless of the values assumed by the lower comfort band, while
 406 on the other hand, only for the maximum value of the lower comfort band ($\Delta T_{sp, min, DR}$ equal to 2 °C) the event can be
 407 realized for each value greater than 0 °C of the upper comfort band. This behavior is also confirmed by the trend of
 408 $E_{shift, bDR}$ (Figure 10(b)). Indeed, for the higher values of the upper comfort band ($\Delta T_{sp, max, DR}$ from 0.8 °C to 1 °C)
 409 overconsumptions of less than 30 % are obtained (regardless of the value of the lower comfort band), on the other
 410 side, when high values of the lower comfort band ($\Delta T_{sp, min, DR}$) are allowed with low values of the upper comfort band
 411 ($\Delta T_{sp, max, DR}$), significant overconsumption must be expected ($E_{shift, bDR}$ greater than 40 % for $\Delta T_{sp, max, DR}$ lower than 0.6
 412 °C). However, the high involvement of the flexibility derived by TCLs in the hours before the peak reduction event
 413 positively affects the building response in the time after the event, as can be seen in Figure 10(c). Indeed, it can be
 414 noticed that as the $\Delta T_{sp, max, DR}$ decreases, regardless of the $\Delta T_{sp, min, DR}$, it increases the energy savings after the event
 415 ($E_{shift, aDR}$). This behavior suggests that the optimal solution evaluated to realize the event and to minimize the thermal
 416 demand aims to take advantage of the precooling also for the hours after the event.

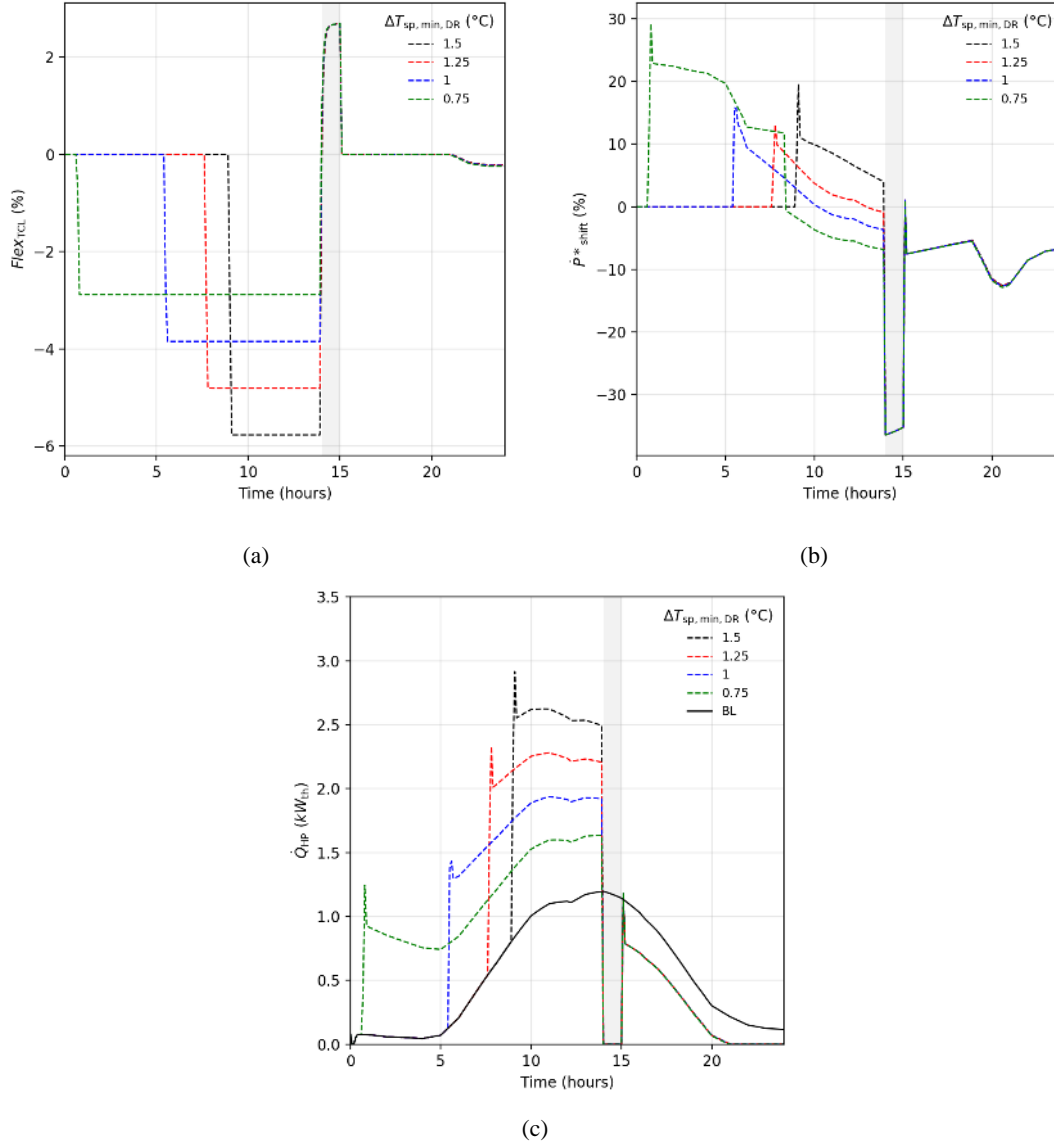


417 **Figure 10.** Daily flexibility curves for an event with f_{PS} equal to 0 (100% peak reduction) and Δk_{DR} of 1 hour as the $\Delta T_{sp,max,DR}$
 418 and $\Delta T_{sp,min,DR}$ vary for FCU (without TES): (a) Pre-cooling of the internal air node duration (Δk_{prec}), (b) $E_{shift,bDR}$ and (c) $E_{shift,aDR}$.

419

420 It is interesting to notice that, while for each value of the upper comfort band (for example $\Delta T_{sp,max,DR}$ equal to 0.7 °C)
 421 the duration of pre-cooling (Figure 10(a)) increases as the lower comfort band ($\Delta T_{sp,min,DR}$) decreases, $E_{shift,bDR}$
 422 decreases with the lower comfort band (pre-cooling requires less heat to be removed). However, $E_{shift,bDR}$ reaches a
 423 minimum at a certain value of the lower comfort band (at $\Delta T_{sp,min,DR}$ of 1 °C for the curve relative to $\Delta T_{sp,max,DR}$ 0.7
 424 °C in Figure 10(b)), then it starts to rise again. This is due to the fact that for small values of the lower comfort band

425 ($\Delta T_{sp,min,DR}$ below 1 °C), very long pre-cooling times are required which greatly affect the electricity consumption.
 426 This behavior is confirmed by the curves in Figure 11: the thermal capacity of the heat pump decreases in power and
 427 increases in time when the lower comfort band decreases (Figure 11(c)). However, it is not translated in the same
 428 monotonous trend of the power (\dot{P}_{shift}^* in Figure 11(b)) because of the nonlinear variation of the *EER* with the working
 429 conditions. In Figures 11(b) and (c) it can be also noticed the lowering of the electrical and the thermal demand in the
 430 hours after the event that can be obtained thanks to the exploitation of the pre-cooling.



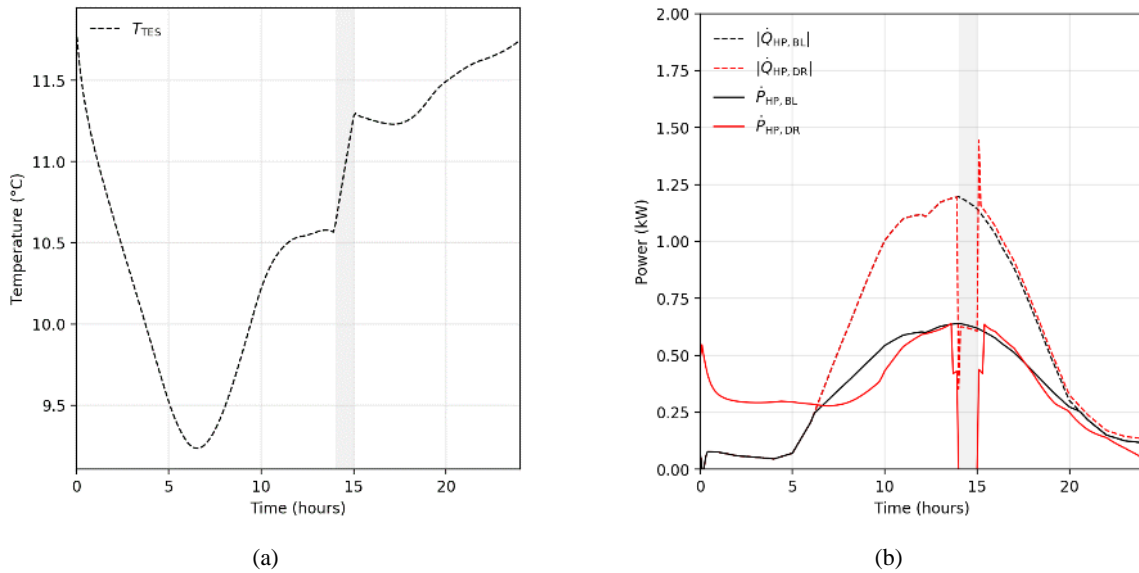
431 **Figure 11.** Daily Demand Response operation (f_{PSS} equal to 0, Δk_{DR} of 1 hour, $\Delta T_{sp,max,DR}$ of 0.7 °C and with variable $\Delta T_{sp,min,DR}$)
 432 for FCU (without TES): (a) *FlexTCL*, (b) \dot{P}_{shift}^* and (c) thermal power of the HP.

433
 434 In APPENDIX A the flexibility curves with different peak reductions are reported. As expected, the flexible behavior
 435 of the system is the same as discussed for the previous case (f_{PSS} equal to 0) with a scaled trend (i.e., as the peak
 436 reduction decreases both the duration of the pre-cooling phase, Δk_{prec} , and the electricity consumption variation before
 437 the event, $E_{s\text{hit},bDR}$, decrease, while the electricity saving after it, $E_{s\text{hit},aDR}$, increases). In any case, in all the tested
 438 configurations of peak shaving (see APPENDIX A) it is clear that, a high involvement of the user (in term of setpoint
 439 variations) has to be taken into account when no thermal inertia is available, especially to produce high electricity
 440 consumption reductions. Anyhow, if a large variation of the setpoint is allowed during the event (minimum $\Delta T_{sp,max,DR}$

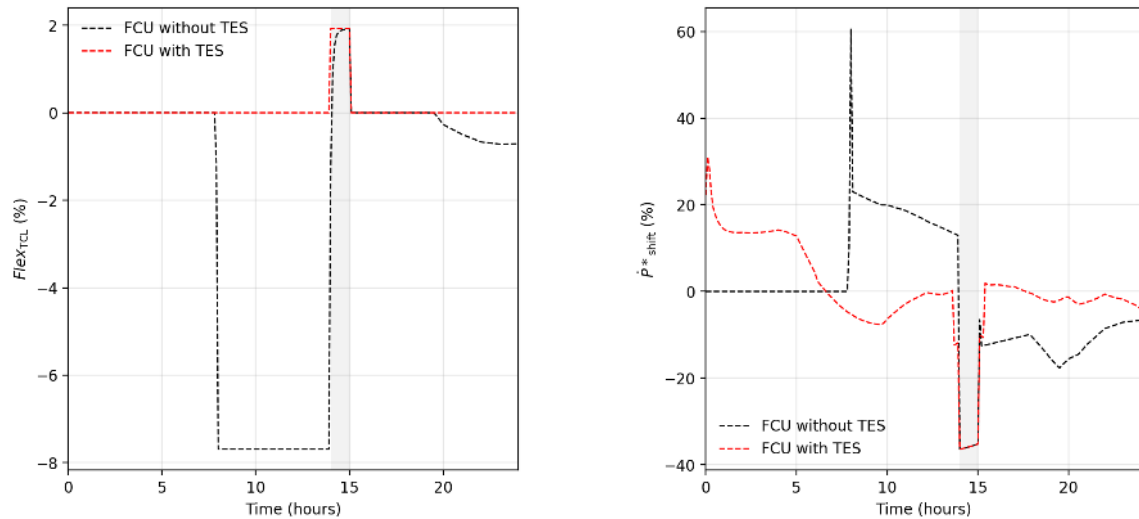
441 of 1 °C), the system, due to the rapidity of the variation, allows to realize all the required consumption reductions,
 442 with low values of pre-cooling time (lower than 2.25 hours).

443 Hence, it is possible to conclude that when there is no thermal inertia, the possible demand variation produced by
 444 exploiting the TCLs is limited and, where possible, it consistently affects the users comfort conditions. On the
 445 contrary, if a TES is added to the water circuit of the fan coil, its thermal inertia allows to realize different types of
 446 Demand Response events even without setpoint temperature modifications. In Figure 12 the same peak reduction of
 447 Figures 7 and 9 realized in the configuration with the TES is shown. In this case the flexibility from TCLs before the
 448 event is not exploited (Δk_{prec} is equal to 0 hours) and the cooling power stored in the TES is used during the event
 449 (Figure 12(b)). Moreover, also a lower $E_{\text{shift,BDR}}$ is calculated. It is + 23 % in case of FCU with TES in comparison to
 450 + 46 % in the configuration without the TES.

451 In order to highlight the role of the TES, Figure 13 represents the comparison between the flexibility evaluation
 452 parameters ($Flex_{\text{TCL}}$ and \dot{P}_{shift}^*) for the FCU system with and without the presence of the TES: also considering the
 453 most extreme case treated ($\Delta T_{\text{sp,min,DR}}$ equal to 0.5 °C and $\Delta T_{\text{sp,max,DR}}$ equal to 0 °C), a $Flex_{\text{TCL}}$ of 0 % is calculated
 454 throughout the day (Δk_{prec} of 0 hours) in presence of TES.

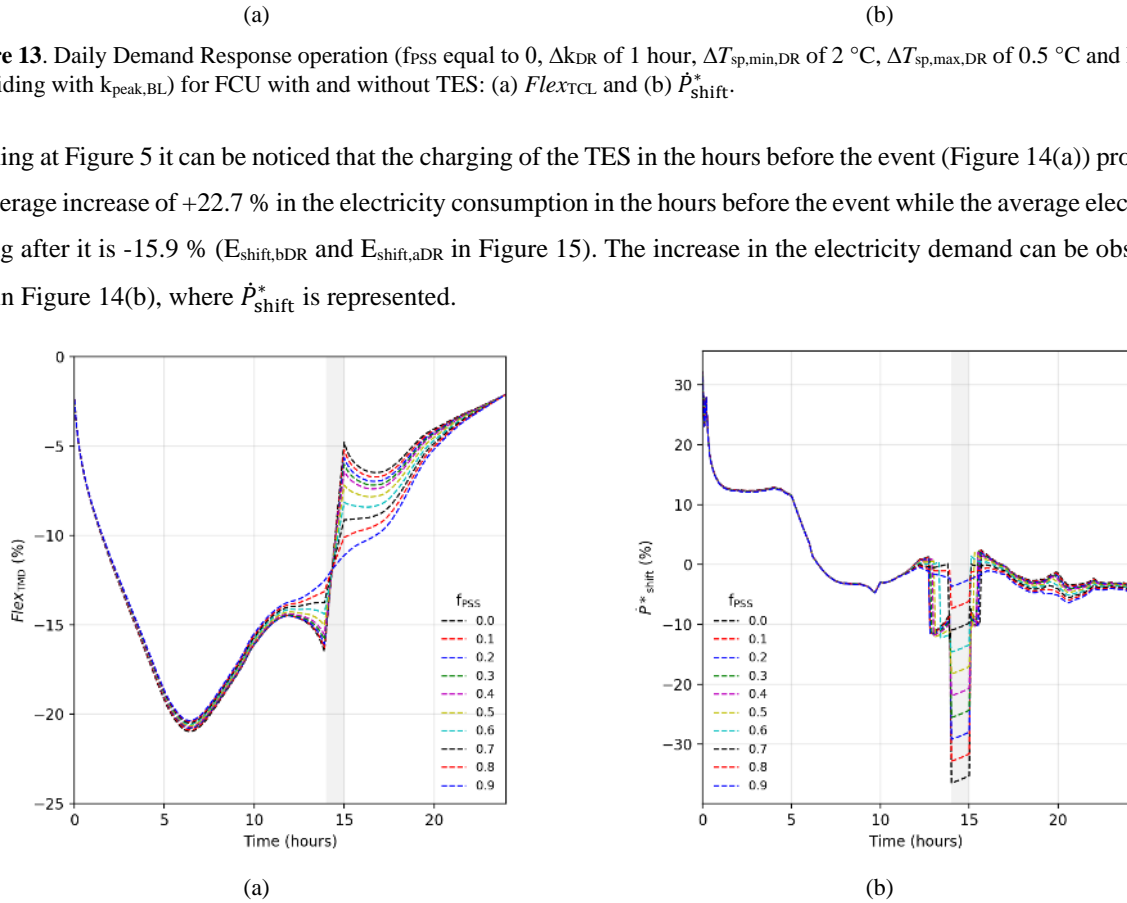


455 **Figure 12.** Daily comparison between BL and DR event (f_{PSS} equal to 0, Δk_{DR} of 1 hour, $\Delta T_{\text{sp,min,DR}}$ of 2 °C, $\Delta T_{\text{sp,max,DR}}$ of 0.5 °C
 456 and $k_{\text{start,DR}}$ coinciding with $k_{\text{peak,BL}}$) for FCU with TES: (a) TES node temperature and (b) thermal and electrical power of the heat
 457 pump.

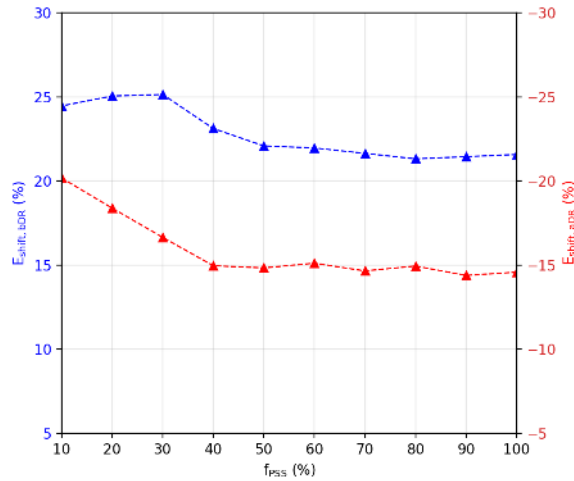


458 **Figure 13.** Daily Demand Response operation (f_{PSS} equal to 0, Δk_{DR} of 1 hour, $\Delta T_{sp,min,DR}$ of 2 °C, $\Delta T_{sp,max,DR}$ of 0.5 °C and $k_{start,DR}$
 459 coinciding with $k_{peak,BL}$) for FCU with and without TES: (a) $Flex_{TCL}$ and (b) \dot{P}_{shift}^* .
 460

461 Looking at Figure 5 it can be noticed that the charging of the TES in the hours before the event (Figure 14(a)) produces
 462 an average increase of +22.7 % in the electricity consumption in the hours before the event while the average electricity
 463 saving after it is -15.9 % ($E_{shift,bDR}$ and $E_{shift,aDR}$ in Figure 15). The increase in the electricity demand can be observed
 464 also in Figure 14(b), where \dot{P}_{shift}^* is represented.



465 **Figure 14.** Daily Demand Response operation (Δk_{DR} of 1 hour, $\Delta T_{sp,max,DR}$ of 0 °C and $\Delta T_{sp,min,DR}$ of 0.5 °C) for FCU with TES as
 466 the f_{PSS} varies: (a) $Flex_{TMD}$ and (b) \dot{P}_{shift}^* .



467 **Figure 15.** Daily flexibility curve related to $E_{shift,bDR}$ and $E_{shift,aDR}$ (Δk_{DR} of 1 hour, $\Delta T_{sp,max,DR}$ of 0 °C and $\Delta T_{sp,min,DR}$ of 0.5 °C) for
 468 FCU with TES as the f_{PSS} varies.
 469

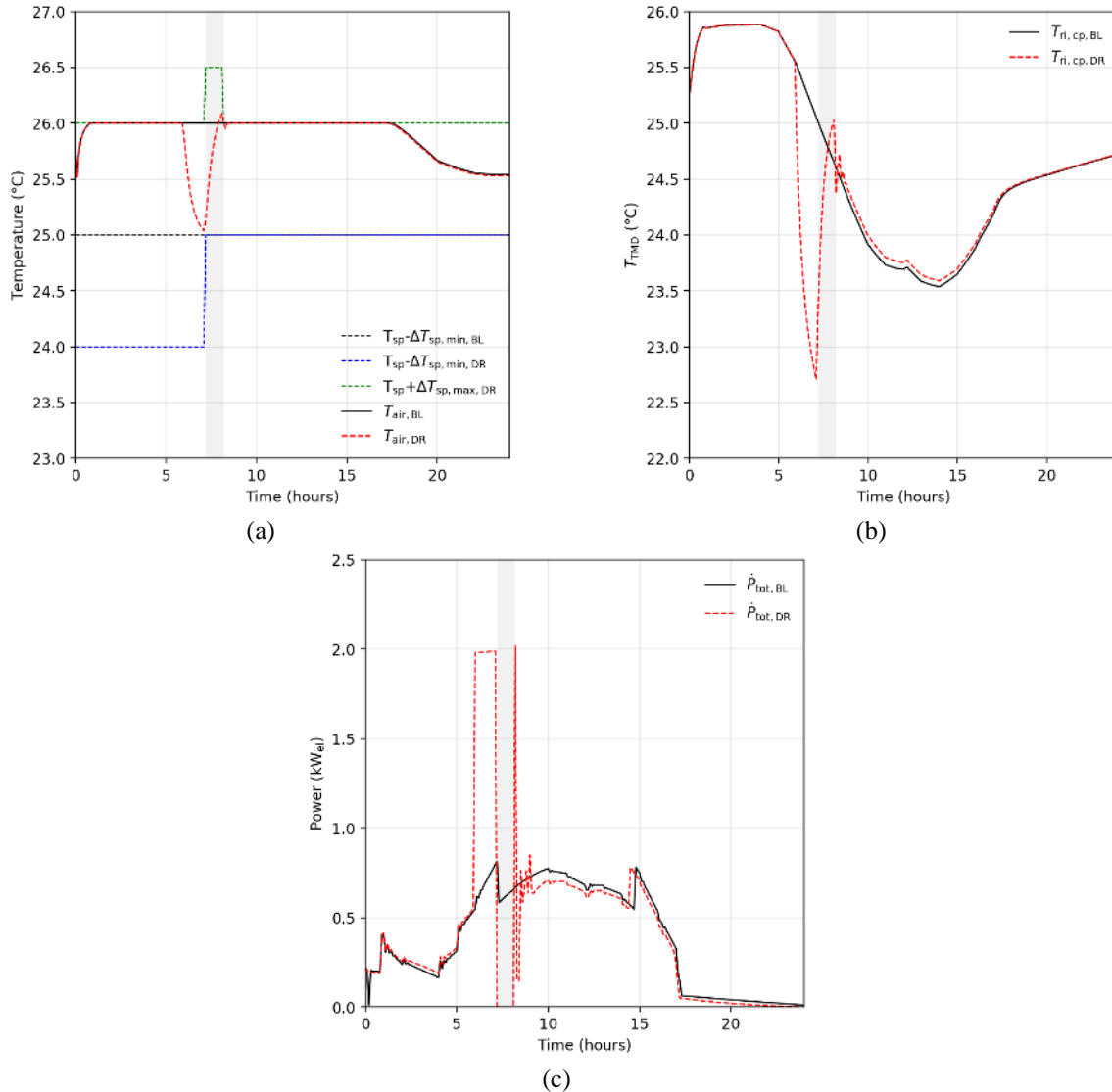
470 On the basis of these results it is therefore possible to conclude that, for the FCU system, the only way to produce
 471 different events without involving the end user's thermostat is to provide a thermal storage system (i.e., FCU with
 472 TES). Indeed, if the TES is added to the FCU distribution system, its thermal mass contribution (the temperature T_{TES}
 473 represents the temperature of the TMD) allows to implement all the peaks reduction so far discussed without any
 474 involvement of the air node setpoint temperature.
 475

476
 477

478 4.1.3 Ceiling panels (CP) with dehumidifier (DH)

479 In the ceiling panels system (CP) the sensible cooling power provided by the heat pump is not removed directly from
 480 T_{air} but it is provided to the inner layer of the roof ($T_{ri,cp}$ in Figure 3). From this decoupling, a minimum level of thermal
 481 inertia can be derived by the mass of the envelope and the system is able to realize differently the peak shaving events
 482 with also minimum variations of the comfort bands (i.e., $\Delta T_{sp,min,DR}$ and $\Delta T_{sp,max,DR}$).

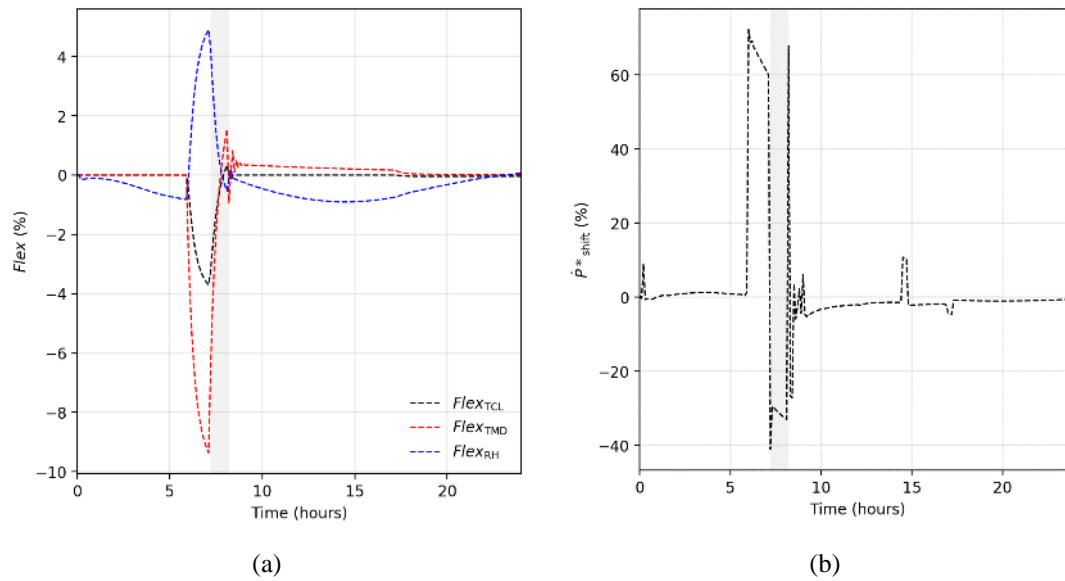
483 Focusing on an event that imposes a 100 % peak reduction (f_{PSS} equal to 0), in the same conditions tested in the
 484 previous sections (Δk_{DR} of 1 hour, $\Delta T_{sp,min,DR}$ of 2 °C, $\Delta T_{sp,max,DR}$ of 0.5 °C and $k_{start,DR}$ coinciding with $k_{peak,BL}$), the
 485 comparison between the Demand Response event and the Baseline is shown in Figure 16.



486 **Figure 16.** Daily comparison between BL and DR event (f_{PSS} equal to 0, Δk_{DR} of 1 hour, $\Delta T_{sp,min,DR}$ of 2 °C, $\Delta T_{sp,max,DR}$ of 0.5 °C,
 487 $\Delta RH_{sp,min,DR}$ of 5 %, $\Delta RH_{sp,max,DR}$ of 5 % and $k_{start,DR}$ coinciding with $k_{peak,BL}$) for CP: (a) air node; (b) roof node temperatures and
 488 (c) electrical consumption (HP and DH).
 489

490 In this case, since the cooling system is also equipped with a dehumidifier to control the indoor relative humidity, the
 491 electricity peak time is estimated on the total electricity consumption curve (DH and HP). In particular the peak (in
 492 Baseline) occurs at 7.20 am with a value of 0.82 kW_{el} (of which 14.6 % is derived from the dehumidifier and the
 493 remaining 85.4 % from the heat pump). The total electricity consumption is 9.2 kWh_{el}, 75 % of that is produced by
 494 the HP and the remaining 25 % by the DH.

495 Looking at the red curves in Figures 16(a) and (b) which represent the results of the Demand Response event, it can
 496 be noted that, thanks to the thermal mass of the roof layer, the CP system allows a low exploitation of TCLs. Indeed,
 497 the pre-cooling is about 1.2 hours. However, to cool down $T_{i,cp}$, the anticipated overconsumption of the heat pump is
 498 significantly higher (Figure 16(c)) with a $E_{shift,bDR}$ of 67 % (the \dot{P}_{shift}^* curve (Figure 17(b)) reaches values of 72 %
 499 during the precooling phase). Figure 17(a) shows the dynamic involvement of each energy flexibility source (i.e.
 500 flexibility of the thermostatically controlled loads, thermal mass and relative humidity variation) for the tested event.
 501 In particular, for the relative humidity flexibility parameter ($Flex_{RH}$), it can be noted that during the peak shaving
 502 event, $Flex_{RH}$ decreases while it increases in the preceding hours. However, this is not derived by an optimized control
 503 logic, but it is a simple consequence of the internal temperature trend (T_{air}). Therefore, the flexibility linked to the
 504 variation of the relative humidity is strictly dependent on the temperature variation.
 505



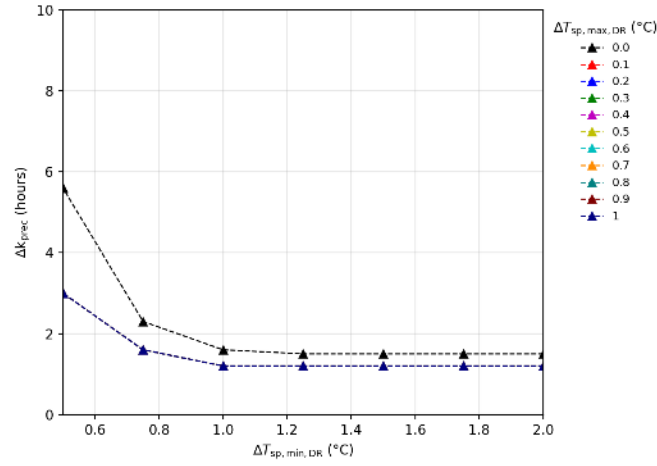
506 **Figure 17.** Daily Demand Response operation (f_{PSS} equal to 0, Δk_{DR} of 1 hour, $\Delta T_{sp,min,DR}$ of 2 °C, $\Delta T_{sp,max,DR}$ of 0.5 °C, $\Delta RH_{sp,min,DR}$
 507 of 5 %, $\Delta RH_{sp,max,DR}$ of 5 % and $k_{start,DR}$ coinciding with $k_{peak,BL}$) for CP: (a) $Flex_{TCL}$, $Flex_{TMD}$ and $Flex_{RH}$ and (b) \dot{P}_{shift}^* .
 508

509 Thanks to the involvement of both the TMD and the TCLs in the ceiling panels system, the configurations in which
 510 the events are not feasible decrease considerably. As showed in the flexibility curves of Figure 18, in which a peak
 511 annulment (f_{PSS} of 0 for 1 hour) is tested in different conditions of temperature setpoint limits, the optimization
 512 problem finds a feasible solution for each combination of the comfort bands ($\Delta T_{sp,max,DR}$ and $\Delta T_{sp,min,DR}$). However,
 513 focusing on the cases shown in Figure 18, a lower influence of the comfort limits on the realization of the event in CP
 514 may be noted. In particular, only the lowest values of the comfort bands ($\Delta T_{sp,min,DR}$ under 1 °C) produce a worsening
 515 of performance in term of Δk_{prec} (Figure 18(a)).

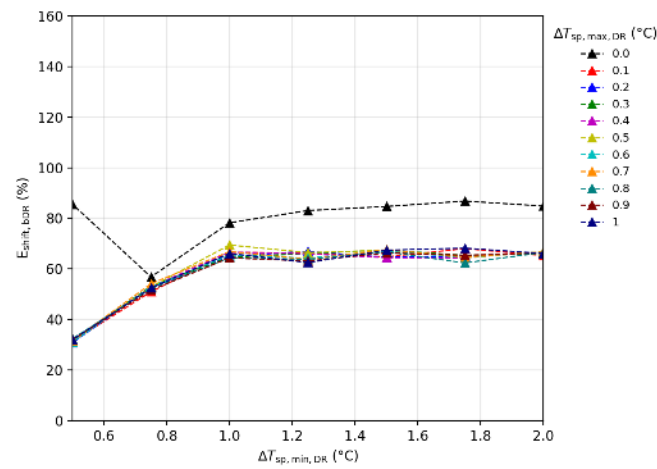
516 In the other cases ($\Delta T_{sp,min,DR}$ greater than 1 °C), similar values of Δk_{prec} and $E_{shift,bDR}$ are calculated regardless the
 517 values assumed by the comfort limits. Looking at Figure 18(c) it can be noticed that, also in this case the pre-cooling
 518 allows to produce a lowering of the electricity demand also in the hours after the event.

519 Moreover, no influence of the parameter $\Delta RH_{sp,max,DR}$ and $\Delta RH_{sp,min,DR}$ is observed (APPENDIX B).

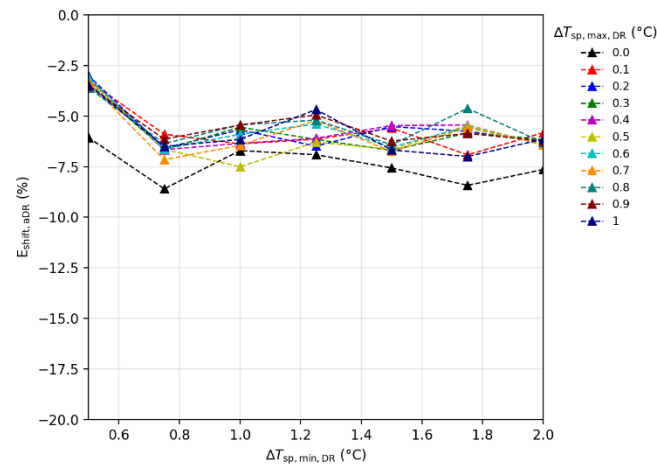
520
 521
 522
 523



(a)



(b)



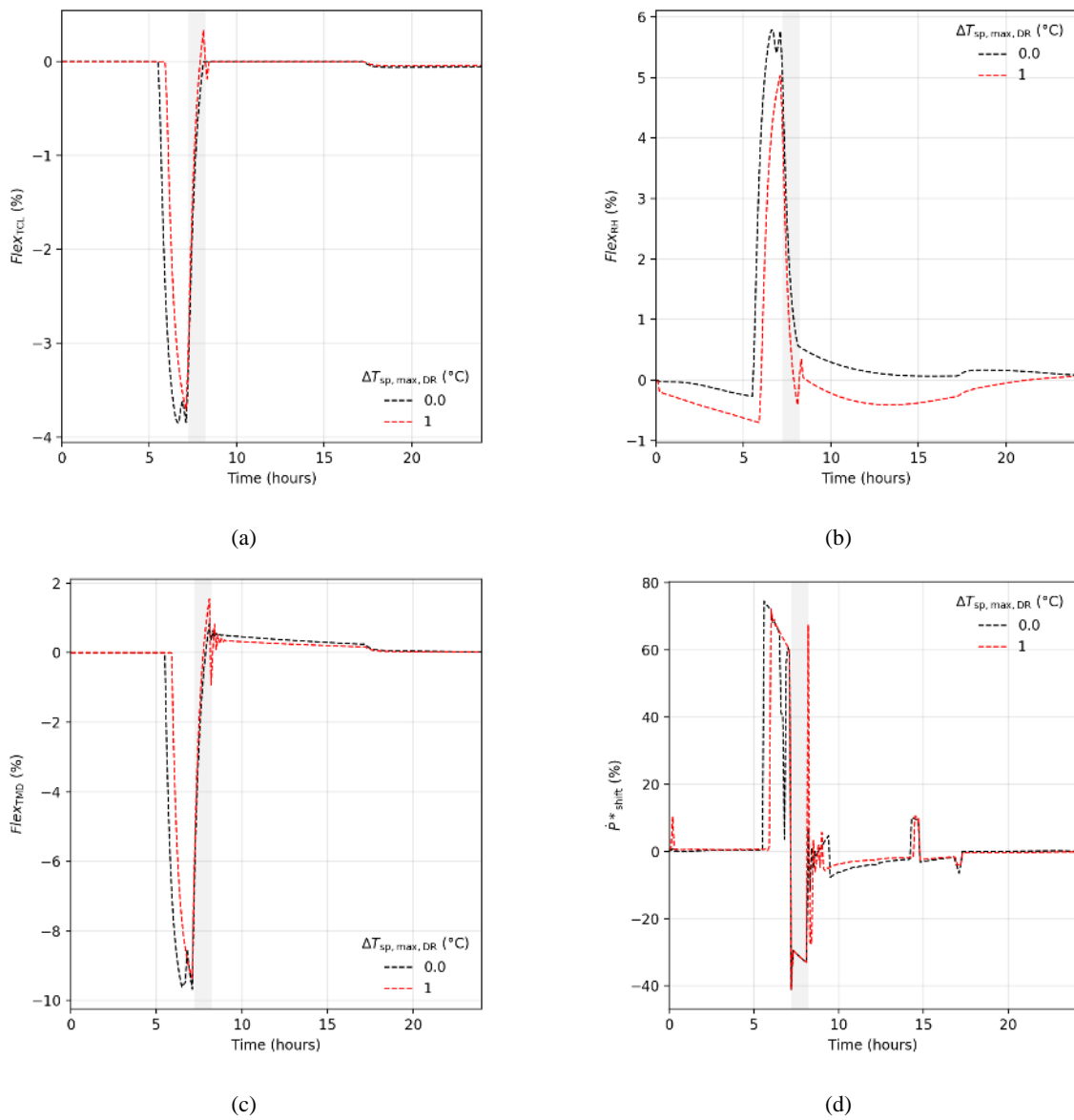
(c)

524 **Figure 18.** Daily flexibility curves for an event with f_{PS} equal to 0 (100% peak reduction) and Δk_{DR} of 1 hour as the $\Delta T_{sp,max,DR}$
 525 and $\Delta T_{sp,min,DR}$ vary for CP ($\Delta RH_{sp,min,DR}$ and $\Delta RH_{sp,max,DR}$ equal to 5 %): (a) Pre-cooling of the internal air node duration (Δk_{prec}),
 526 (b) $E_{shift,bDR}$ and (c) $E_{shift,aDR}$.

527

528 In Figure 19, the dynamic comparison between the case in which the 100 % peak reduction is produced with the lowest
 529 and the greatest values of the upper comfort band ($\Delta T_{sp,max,DR}$ respectively 0 °C and 1°C) with a fixed values of 1 °C
 530 for the lower comfort band $\Delta T_{sp,min,DR}$ is shown. Looking at Figure 19(d) it can be immediately noted the high peak
 531 values reached by the \dot{P}_{shift}^* curves (near 80%) in the time before the event in both configurations. In particular, in

532 case of upper comfort band ($\Delta T_{sp,max,DR}$ equal to 1 °C (red curves in Figure 19) also a peak in the \dot{P}_{shift}^* after the event
533 occurs although the overall consumption decreases in the hours following the event ($E_{shift,aDR}$ in Figure 18(c)).
534 Moreover, due to the storage capability of the ceiling panels and its slower speed in following precise variations in
535 the internal temperature (heat is not removed directly from T_{air}), even with a $\Delta T_{sp,max,DR}$ of 1 °C, the internal
536 temperature takes the entire duration of the event (Δk_{DR}) to rise (Figure 19(a)) up to 26.1 °C (not all the allowed
537 $\Delta T_{sp,max,DR}$ is exploited). Looking at Figure 19(b), a variation of $Flex_{RH}$ can be appreciated. However, as mentioned, it
538 is only a consequence of the sensitive cooling of the internal air in the precooling. In Figure 19(c) instead, the
539 utilization of the flexibility of the thermal mass of the distribution system ($Flex_{TMD}$) is represented. Because of the
540 low thermal inertia of the $T_{ri,cp}$ node, the latter has the same trend of $Flex_{TCL}$. However, $Flex_{TMD}$ reaches twice as low
541 values as during the pre-cooling phase. This is the reason why high overconsumption are evaluated (Figures 18(b) and
542 19(d)). Similar behaviors can be observed for lower peak reductions (f_{PSS} greater than 0) as showed in APPENDIX B.

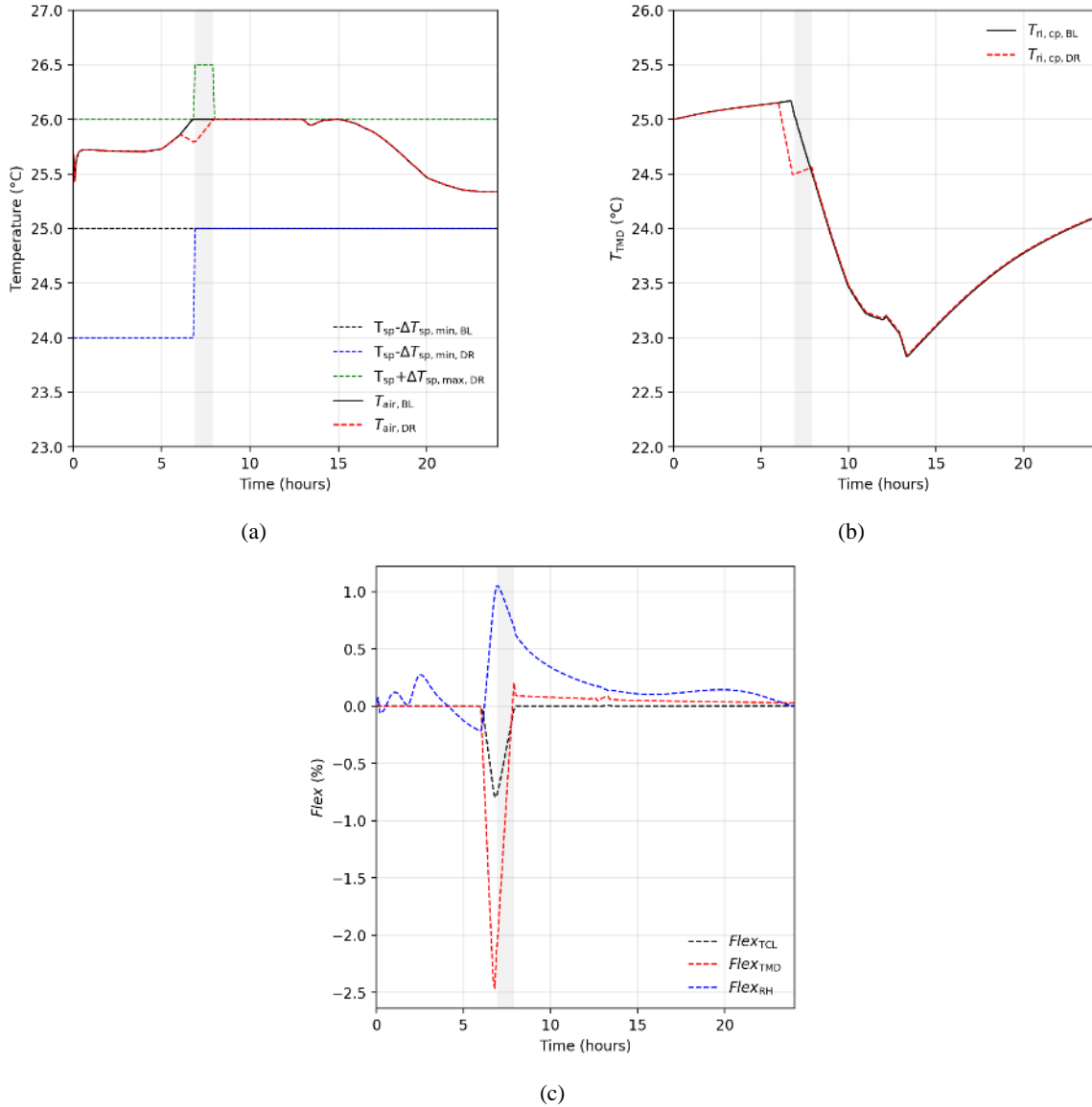


543 **Figure 19.** Daily Demand Response operation (f_{PSS} equal to 0, Δk_{DR} of 1 hour, $\Delta T_{sp,max,DR}$ of 0 °C and 1 °C and $\Delta T_{sp,min,DR}$ of 1 °C)
544 for CP: (a) $Flex_{TCL}$, (b) $Flex_{RH}$, (c) $Flex_{TMD}$ and (d) \dot{P}_{shift}^* .

545
546

547 4.1.4 Cooling concrete ceiling (CC) with dehumidifier (DH)

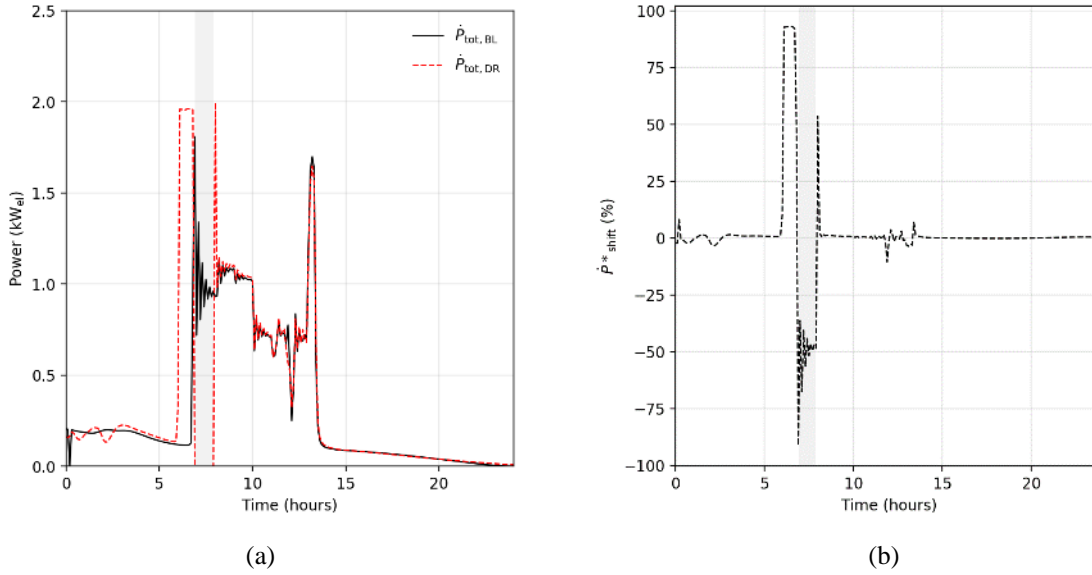
548 When the cooling power of the heat pump is removed from a high massive node, as in case of concrete ceiling cooling
 549 system (CC), the Demand Response event analyzed for the previous cases (f_{PSS} equal to 0 for Δk_{DR} of 1 hour) can be
 550 implemented with a low involvement of the TCLs flexibility. Indeed, the high storage capability of the roof node (T_{ri}
 551 in Figure 2) allows to keep the air temperature near to the setpoint of 26 °C (Figure 20(a)) during the event at the
 552 expense of a pre-cooling of the thermal mass of the distribution system (Figure 20(b)).



553 **Figure 20.** Daily Demand Response operation (f_{PSS} equal to 0, Δk_{DR} of 1 hour, $\Delta T_{sp, min, DR}$ of 2 °C, $\Delta T_{sp, max, DR}$ of 0.5 °C, $\Delta RH_{sp, min, DR}$
 554 of 5 %, $\Delta RH_{sp, max, DR}$ of 5 % and $k_{start, DR}$ coinciding with $k_{peak, BL}$) for CC: (a) air node temperature, (b) roof node temperature and
 555 (c) $Flex_{TCL}$, $Flex_{TMD}$ and $Flex_{RH}$.

556 Although the variation of the temperature of the thermal mass node (T_{ri}) is relatively small ($Flex_{TMD}$ reaches the
 557 minimum value of - 2.5 % in Figure 20(c)), the large thermal inertia of the cooling system involves a not negligible
 558 increase in the power curve (Figure 21). Indeed, due to the high involvement of the thermal inertia of the distribution
 559 system, the estimated increase of electricity consumption before the peak shaving event becomes 116 % ($E_{shift, bDR}$)
 560 with a peak of almost 100 % in the \dot{P}_{shift}^* curve (Figure 21(b)). In this case, also the electricity consumption after the
 561

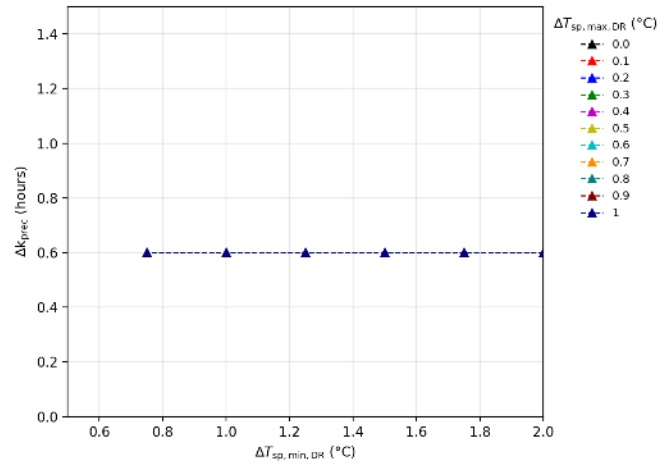
562 event increases (1.24 % of $E_{\text{shift,aDR}}$). Indeed, a peak power can be observed even immediately after the event (Figure
 563 21).
 564 It is important to highlight that in this case, as for CP, also the relative humidity is controlled by the cooling system
 565 with a dehumidifier and the power curves showed in Figures 21(a) and (b) take into account both contributions. The
 566 trend of the parameter $Flex_{RH}$ (Figure 20(c)) shows again its dependence on the temperature, which has a prevalent
 567 impact on the achievement of the comfort limits.



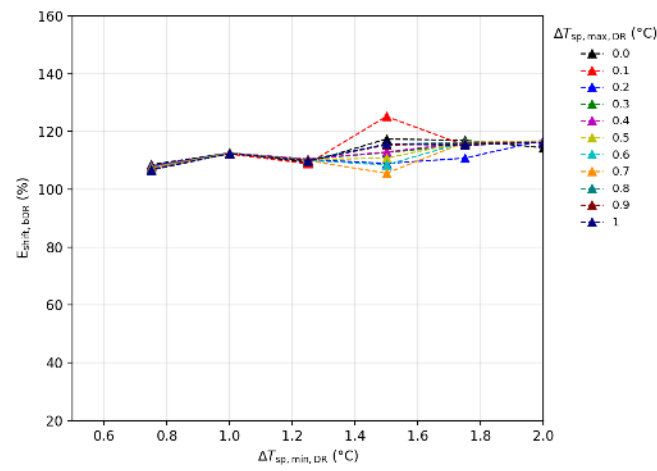
568 **Figure 21.** Daily Demand Response operation (f_{PSS} equal to 0, Δk_{DR} of 1 hour, $\Delta T_{\text{sp,min,DR}}$ of 2 °C, $\Delta T_{\text{sp,max,DR}}$ of 0.5 °C, $\Delta RH_{\text{sp,min,DR}}$
 569 of 5 %, $\Delta RH_{\text{sp,max,DR}}$) for CC: (a) electrical consumption (HP and DH) and (b) \dot{P}_{shift}^* .
 570

571 In Figure 22, the flexibility curves in case of 100 % peak reduction in different conditions of comfort bands are
 572 showed, while Figure 23 represents the dynamic flexible behavior in the same cases with a focus on a fixed value of
 573 the lower comfort band ($\Delta T_{\text{sp,min,DR}}$ equal to 1 °C).

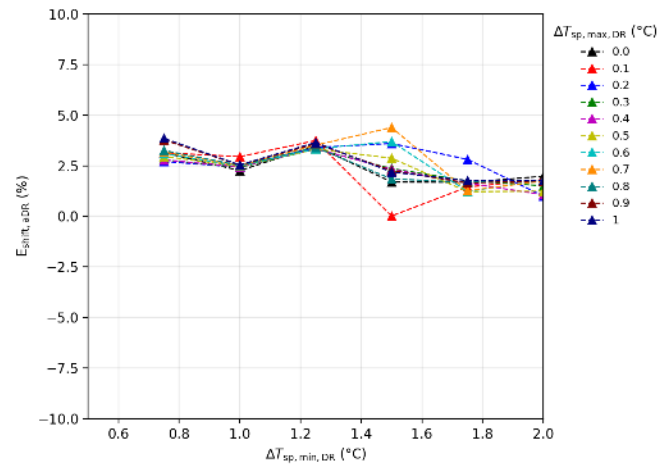
574 Looking at Figure 23(a) it can be noted that during the event the upper comfort range ($\Delta T_{\text{sp,max,DR}}$) is not exploited and
 575 $Flex_{\text{TCL}}$ does not reach the value - 1 % in the time before the event. Therefore, albeit a precooling time of 0.6 hours
 576 (Δk_{prec} in Figure 22(a)) is measured, it does not correspond to an effective exploitation of the lower flexibility band
 577 ($\Delta T_{\text{sp,min,DR}}$). On the contrary, considering the large thermal mass of the CC system, the flexibility of the thermal mass
 578 of the distribution system is more involved ($Flex_{\text{TMD}}$ reaches the value of - 2.5 %, Figure 23(c)). This is also the
 579 reason why a higher increase in the electricity power consumption is obtained (Figures 22(b) and 23(d)). It is
 580 interesting to notice that, when a large thermal inertia is involved to realize the event, even a delayed power peak after
 581 the event is always observed (Figure 23(d)) and the electricity consumption after the event is always greater than 0 %
 582 (Figures 22(c)).



(a)

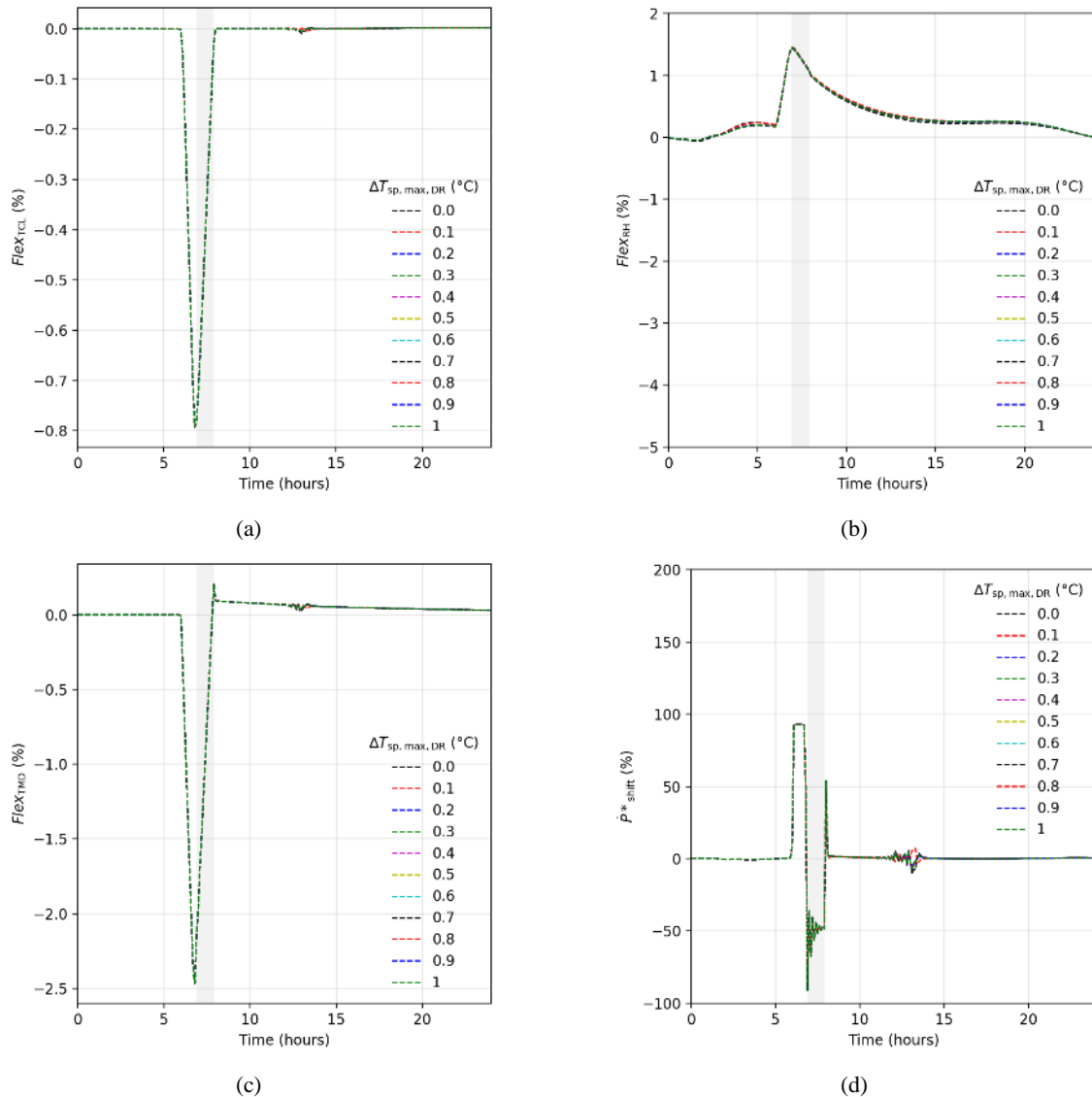


(b)



(c)

583 **Figure 22.** Daily flexibility curves for an event with f_{ps} equal to 0 (100 % peak reduction) and Δk_{DR} of 1 hour as the $\Delta T_{sp,max,DR}$
 584 and $\Delta T_{sp,min,DR}$ vary for CC ($\Delta RH_{sp,min,DR}$ and $\Delta RH_{sp,max,DR}$ equal to 5 %): (a) Pre-cooling of the internal air node duration (ΔK_{prec}),
 585 (b) $E_{shift,bDR}$, and (c) $E_{shift,aDR}$.



586 **Figure 23.** Daily Demand Response operation (f_{PSS} equal to 0, Δk_{DR} of 1 hour, $\Delta T_{sp,max,DR}$ varies and $\Delta T_{sp,min,DR}$ of 1 °C) for CC:
 587 (a) $Flex_{TCL}$, (b) $Flex_{RH}$, (c) $Flex_{TMD}$ and (d) P^*_{shift} .

588
 589 More flexibility curves about the CC systems are reported in APPENDIX C, where a focus on different peak
 590 reductions values is also provided. Looking at the flexibility curves reported in APPENDIX C, it can be noted that the
 591 behavior of the cooling concrete ceiling plant (CC) in producing a certain peak reduction is quite independent on the
 592 Demand Response parameters. This is due to the fact that, the storage capacity of the distribution system (TMD) is
 593 mostly used. In particular, it is interesting to notice that for peak reductions lower that 60 %, the CC system allows to
 594 avoid almost entirely the involvement of the flexibility derived by TCLs regardless of the values assumed by limits
 595 granted to the thermostat.

596 To conclude, it is possible to observe that when the heat is accumulated in a high massive layer of the building
 597 envelope (e.g., the roof), different peak shaving events can be performed thus limiting the effect on the indoor
 598 temperature to a minimum. On the contrary, large over energy consumption are expected, both before and after the
 599 event.

600
 601
 602

603 **4.2 Comparison between the Space Cooling systems**

604 The presented analysis demonstrates that Space Cooling technologies differ in terms of type and entity of exploitation
605 of different flexibility resources (i.e. the involvement (i) of the thermostatic controlled loads or (ii) of the thermal
606 inertia of the distribution system) with different consequences on the electric power curve (i.e. presence of payback
607 loads) during peak shaving events.

608 As far as the split systems are concerned, they are the most inflexible systems among those analyzed. Indeed, as it
609 does not allow any modulation of the heat pump, the split can realize only a Demand Response event with a reduction
610 factor (f_{PSS}) equal to zero. Moreover, a high involvement of the user's temperature setpoint is necessary, not having
611 any thermal inertia available. Another important aspect that can be noticed by observing the split power curves (Figure
612 7) involves the difficulty in predicting the trend of the electricity demand in the period before and after the event. This
613 last point, due to the cycling of the heat pump, differentiates the behavior of this technology (on-off regulation) from
614 all the other systems modeled. In fact, all the other emission systems (i.e. FCU, CC and CP) are equipped with a
615 variable capacity heat pump which allows a modulation of the load.

616 The fan coil, in its configuration without the TES, as for the split, requires a high involvement of the TCLs (Figure
617 10(a)) because there is no thermal inertia. However, thanks to the load modulation, the FCU can realize a larger
618 number of peak reductions than the split system, even if, as for the SS, the peak power annulment cannot be obtained
619 for each comfort band. Moreover, the variable capacity heat pump affects also the way in which the event is produced.
620 In other words, the limits granted to the setpoint have a great impact in the implementation of the event both in the
621 period before, during and after it. Indeed, if a large variation of the setpoint is allowed during the event (minimum
622 $\Delta T_{sp,max,DR}$ of 1 °C, Figure 10(a)), the FCU, due to its rapidity, can realize all the required consumption reductions
623 with short pre-cooling (lower than 2.25 hours) and low electricity overconsumptions before the event, ($E_{shift,bDR}$ lower
624 than 10 % in Figure 10(b)).

625 A reduced involvement of the user's temperature setpoints can be achieved if a thermal energy storage is added to the
626 fan coil water circuit. In fact, in this case, the exploitation of the thermal inertia of the distribution system produces
627 any peak reductions without modifying the temperature setpoint of the users. This is due to the complete decoupling
628 of demand from generation possible thanks to the storage device added to the plant. On the other hand, although
629 reductions in electrical absorption are achieved after the event (Figure 15), overconsumption must be expected in the
630 moments preceding the event due to the tank charging phase (Figure 15).

631 Therefore, it clearly appears that, even just considering these three types of emission systems (i.e. SS, FCU with and
632 without TES) when the thermal mass available in the thermal distribution system increases, the involvement of the
633 flexibility from TCLs decreases. This behavior is also confirmed by the observation of the results obtained for the
634 massive ceiling systems (i.e. CP and CC). Referring to the same Demand Response event, it can be noted that, thanks
635 to the thermal mass of the roof layer, the CP system requests a lower exploitation of TCLs than the case of the FCU
636 system without the TES both during and before the event. Furthermore, the pre-cooling in the CP is about 81% shorter
637 than the case of FCU. However, to cool down the roof layer of the CP system, the anticipated overconsumption of the
638 heat pump is significantly high ($E_{shift,bDR}$ of + 67 % in case of CP while it is 46 % in case of FCU): $E_{shift,bDR}$ of the CP
639 system is due to a higher electricity power involvement for a shorter period (as showed in Figure 17(b), the \dot{P}_{shift}^*
640 curve reaches values of 72 % during the precooling phase). Nevertheless, albeit to a lesser extent than the FCU without
641 TES (Figure 18(a) in comparison to Figure 10(a)), a certain influence of the comfort limits modification can be
642 observed also on CP systems, because their thermal inertia is limited. On the other hand, the same behavior is not
643 observed for the electricity overconsumption. Indeed, while for the FCU without TES the high involvement of the

644 users' setpoint allows to avoid payback loads, the exploitation of the thermal mass of the CP system does not avoid
645 this effect, regardless of the comfort limits granted (Figure 10(b) in comparison to Figure 18(b)). In particular, for
646 some values of upper comfort band ($\Delta T_{sp,max,DR}$ equal to 1 °C in Figure 19(d)) in the CP system also a peak in the \dot{P}_{shift}^*
647 after the event occurs.

648 To summarize two important aspects can be highlighted.

- 649 • First of all, although with ceiling panels the pre-cooling times are generally lower than in the previous cases (SS
650 and FCU without TES), there is no configuration that allows to carry out a complete reduction of the peak with a
651 pre-cooling lower than 1 hour, which instead happens in the FCU (configuration with the TES or with a high
652 exploitation of the flexibility from TCL).
- 653 • Moreover, especially for the most extreme peak reduction (f_{PSS} equal to 0, 0.1 and 0.2 in APPENDIX B), there is
654 always an increase in electricity consumed before the event ($E_{shift,bDR}$ greater than 0 %), while in the case of FCU
655 it can be almost zero with high involvement of the flexibility from TCLs (APPENDIX A).

656 This difference between these two systems is emphasized when, instead of the CP, a high massive cooling system (i.e.
657 CC) is considered. From the results obtained for concrete ceiling cooling system, it appears that as the thermal inertia
658 level of the node from which the heat is removed increases, the realization of different peak shaving events is possible
659 with the minimum involvement of the flexibility from TCLs. Furthermore, the way in which the events are
660 implemented is almost completely independent on the limits granted to the temperature setpoint (Figure 22). This
661 behavior is similar to that obtained for the FCU in the configuration with TES, even if an important difference in terms
662 of electrical overconsumption and payback loads can be observed between the two systems. The exploitation of a high
663 massive cooling system produces important consequences on the electric power curve both before and after the event.
664 Moreover, even with high levels of thermal mass in the ceiling (as for the CC), a complete decoupling of demand
665 from generation is not possible, thus it is never possible to completely avoid the involvement of users when a peak
666 annulment is required, as it happens with the TES added to the FCU. This aspect must therefore be considered when
667 planning a load management strategy with this type of systems.

668

669 5. CONCLUSIONS

670 Objective of this work was to evaluate qualitatively and quantitatively the operational energy flexibility of the
671 residential space cooling demand. While modelling several technologies (split systems, fan coils with and without
672 TES, ceiling panels, concrete ceiling), attention was paid to the role of the thermal emission systems in the load
673 shifting capability. The systems analyzed represent the most common technologies and are characterized by different
674 sources of flexibility, i.e. the thermal inertial of the system itself or the flexibility provided by the variation of the
675 indoor temperature setpoint (thermostatically controlled loads). In the evaluation, several Demand Response events
676 (i.e., peak shaving strategies) have been tested in comparison with a reference scenario (Baseline). The flexibility
677 potential of each cooling system was evaluated in terms of required variation of the comfort condition of the users
678 (internal temperature and, if possible, relative humidity) and payback loads in the electricity power curve. In particular,
679 flexibility curves have been defined for each plant and they characterize the behavior of individual systems in terms
680 of available flexibility: they quantify the pre-cooling period duration and the energy demand variation during a peak
681 shaving event while varying the temperature comfort band and the peak shaving percentage. The flexibility curves
682 help also to distinguish the different level of involvement of the two main flexibility sources, i.e., thermostatically
683 controlled loads and thermal mass of the distribution system.

684 In this work the flexibility curves for the main technologies involved in the space cooling sector have been provided
685 and the key conclusions derived from their analysis can be summarized as follows:

- 686 • The split system with on-off regulation shows a rather inflexible behavior during peak shaving events. Only peak
687 annulments are possible with a high impact on the users indoor temperature setpoints before the event. In
688 particular, to reduce to zero the electricity consumption in the peak time, a precooling of 2 °C for about 10 hours
689 with an upper comfort band of 0.5 °C have to be adopted and this leads to 28.7 % increment of electricity
690 consumption in the time before the event.
- 691 • Fan coil units coupled with a variable capacity heat pump are the most flexible system when the energy flexibility
692 from thermostatically controlled loads (TCLs) is activated. To avoid great payback loads, it is advisable to allow
693 the internal air temperature to rise during the event. For instance, allowing an increase of 1 °C in the air
694 temperature, the electricity consumption can be reduced of 100 % in the peak time with a very low pre-cooling
695 (from 0.5 to 2.25 hours in relation to the value of the minimum comfort band allowed to the setpoint) and no
696 electricity increase in the time before the event. However, the addition of a thermal energy storage (e.g., a cold-
697 water tank) to the distribution system allows to realize short term peak shaving strategies without compromising
698 the indoor air temperature with low drawback effects in terms of anticipated electricity overconsumptions.
- 699 • As regards high massive cooling system, the storage capability of the distribution system allows the realization
700 of different peak reduction events with a combined exploitation of the energy flexibility derived by
701 thermostatically controlled loads (TCLs) and by its thermal mass. Results show that, as the thermal mass of the
702 system increases (e.g., concrete ceiling cooling in comparison to ceiling panels), the flexibility of the thermostat
703 is less and less exploited. However, increased anticipated overconsumption due to pre-cooling of the thermal
704 mass of the system must be expected: above + 100 % for the concrete ceiling cooling regardless the comfort band,
705 while for ceiling panels it assumes values near to + 35 % with a large comfort band or up to + 80 % for very
706 narrow comfort band. Furthermore, the occurrence of power peaks delayed with respect to the event is also a
707 drawback effect to be expected.
- 708 • When the level of thermal inertia of the emission system decreases, the activation of the energy flexibility from
709 TCLs in the hours before the event allows to obtain also benefits in terms of electricity consumption reduction in
710 the hours following the DR event. Such electricity saving is greater for FCU in the configuration without the TES
711 (a reduction of 96 % can be reached) and decreases passing from CP (maximum energy saving of about 9 %) to
712 CC, where no energy demand reduction occurs after the event.
- 713 • Comparing the flexibility sources exploited by the modelled space cooling systems, it is clear that the TCLs is
714 the only resource available for the split and the FCU systems. The decrease in use of this resource occurs when
715 the thermal inertia of the distribution system increases. Indeed, the exploitation of the TCLs decreases more and
716 more passing by CP to CC at the expense of the thermal mass of the system. However, only in case of an FCU
717 with TES is possible to avoid completely the TCLs exploitation when the electricity peak wants to be annulled.
718 This is due to the decoupling of demand from generation which is only possible with a storage device added to
719 the plant.

720 To conclude, the analysis shows that the type of emission system used to satisfy the cooling demand of a residential
721 building has a considerable impact on how a programmed peak shaving event is handled. Therefore, taking this aspect
722 into consideration, it is of paramount importance to improve the implementation of large-scale DSM strategies
723 involving cooling systems. Indeed, the assessment of the electric power curve variations in the period before and after
724 the event is crucial to plan a strategy by a hypothetical supervisor, diversified on the basis of users expected reactions.

725 At this aim, the introduced flexibility curves have proved to be an easy and fast instrument to summarize the space
 726 cooling dynamic in presence of a peak shaving Demand Response event.

727 NOMENCLATURE

Δk	Timestep (hours)
ΔT	Temperature difference ($^{\circ}\text{C}$)
ΔRH	Relative humidity difference (%)
A	State space model coefficient matrices for state vector
AC	Air cooling
B	State space model coefficient matrices for input
BL	Baseload
C	Thermal capacity (kWh K^{-1})
C	State space model coefficient matrices for state vector
CC	Concrete ceiling
CP	Ceiling panels
<i>CTRL</i>	Boolean control
D	State space model coefficient matrices for input
DH	Dehumidifier
dk	Infinitesimal time difference
DR	Demand Response
DSM	Demand side management
<i>EER</i>	Energy efficiency ratio
f	Reduction factor
FCU	Fan coil unit
Flex	Flexibility curve (%)
\dot{G}	Gains (W)
h	Heat of evaporation ($\text{J kg}_{\text{vap}}^{-1}$)
HP	Heat pump
K	Thermal conductance (W K^{-1})
<i>k</i>	Discrete time (hours)
L	Loss coefficient factor (W K^{-1})
MILP	Mixed -integer linear programming
M	Mass (kg)
\dot{m}	Flowrate (kg s^{-1})
\dot{P}	Electricity power (W_{el})
\dot{P}^*	Electricity power shift (%)
PSS	Peak shaving strategy
\dot{Q}	Thermal power (W_{th})
R	Thermal resistance (K W^{-1})
RH	Relative humidity
SC	Space cooling
SS	Split system
<i>T</i>	Temperature ($^{\circ}\text{C}$)
t	Continuous time (s)
TES	Thermal energy storage
TMD	Thermal mass of the distribution system
U	Input vector
X	State vector

x	Absolute humidity ($\text{kg}_{\text{vap}} \text{kg}_{\text{gas}}^{-1}$)
Y	Output vector

728 SUBSCRIPTS

air	Internal air temperature
aDR	Time after the Demand Response event
bDR	Time before the Demand Response event
BL	Baseline
building	Thermal power to cover building demand
DH	Dehumidifier
DR	Demand Response
end	End time
env	Environment
f	Floor layer
fe	External floor layers
fi	Internal floor layers
fin	Thermal insulation floor layer
full-load	Full load operation
g	Ground
inf	Air infiltrations
int	Internal
l	Thermal losses
max	Maximum
min	Minimum
o	Outdoor
prec	Precooling time
PSS	Peak shaving strategy
rated	Rated conditions
r	Roof layers
re	External roof layers
RH	Relative humidity
ri	Internal roof layers
ri,ap	Internal roof layers (after ceiling panels, outwards)
ri,bp	Internal roof layers (before ceiling panels, inwards)
ri,cp	Internal roof layers (ceiling panels)
rin	Thermal insulation roof layer
s	Solar contribution
SC	Space cooling
shift	Shift power or energy
sp	Setpoint
start	Start time
T	Temperature
TES	Thermal energy storage
TMD	Thermal mass of the distribution system
v	Water vapor
w	Vertical walls layers
we	External vertical walls layers
wi	Internal vertical walls layers
win	Thermal insulation vertical walls floor layer

729

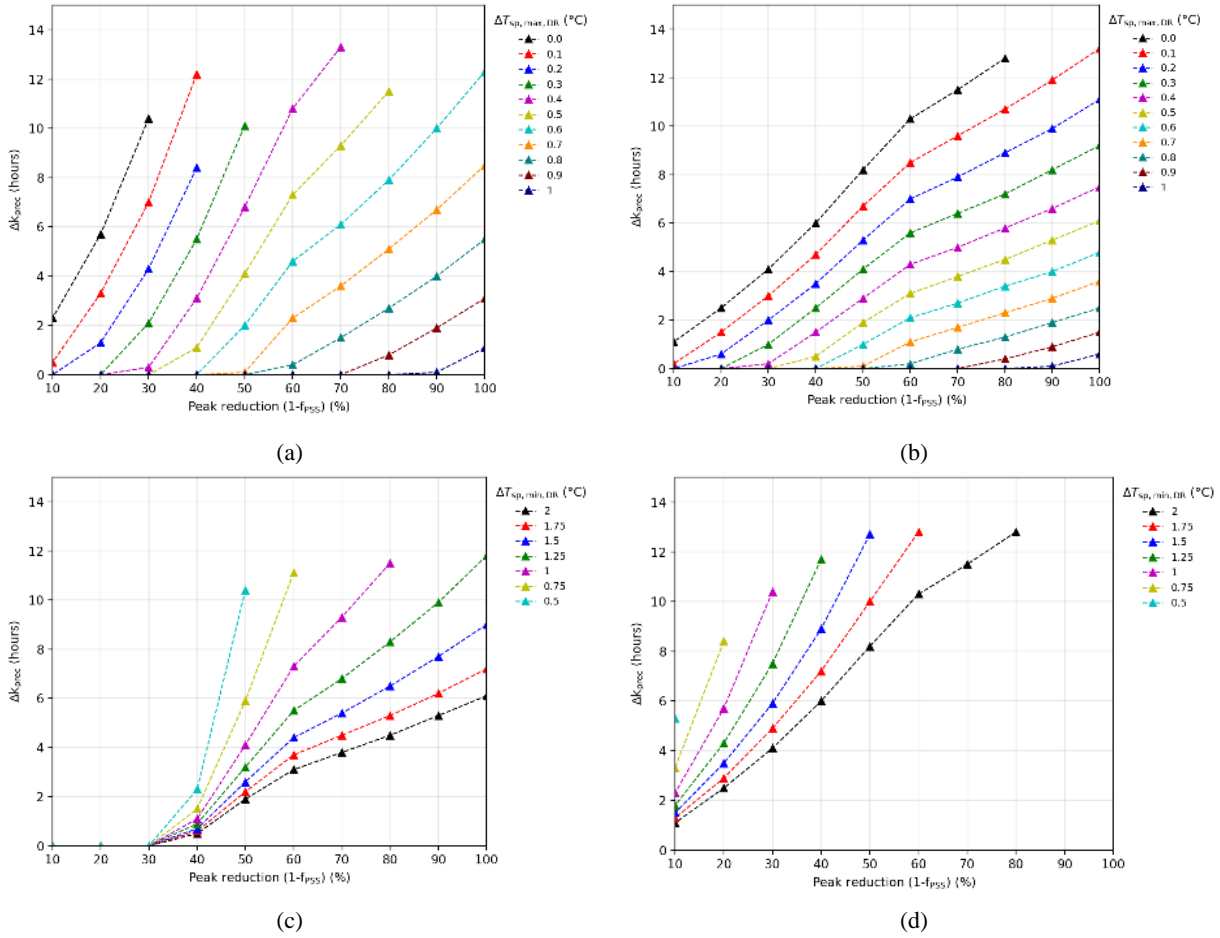
730 **REFERENCES**

731

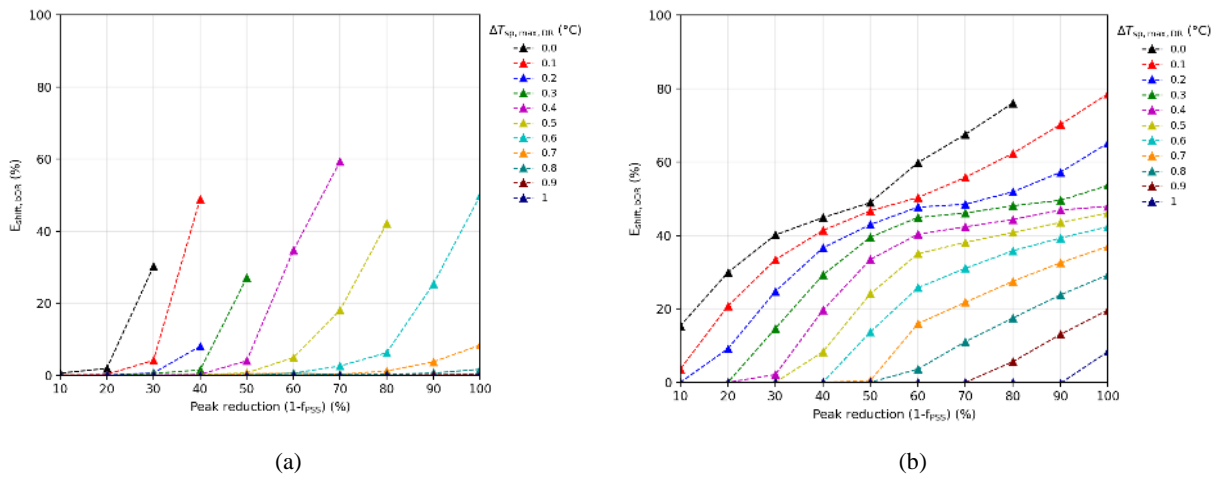
- 732 [1] IEA, Cooling. More efforts needed., Track. Rep. (2020). [iea.org/reports/cooling](https://www.iea.org/reports/cooling) [accessed 7.04.2021].
- 733 [2] IEA, Energy Efficiency Indicators, Stat. Rep. (2020). [iea.org/reports/energy-efficiency-indicators-overview](https://www.iea.org/reports/energy-efficiency-indicators-overview)
734 [accessed 7.04.2021].
- 735 [3] L. Gelazanskas, K.A.A. Gamage, Demand side management in smart grid: A review and proposals for
736 future direction, *Sustain. Cities Soc.* (2014). <https://doi.org/10.1016/j.scs.2013.11.001>.
- 737 [4] N. Oconnell, P. Pinson, H. Madsen, M. Omalley, Benefits and challenges of electrical demand response: A
738 critical review, *Renew. Sustain. Energy Rev.* (2014). <https://doi.org/10.1016/j.rser.2014.07.098>.
- 739 [5] U.S.D. of E. (USDOE), Benefits of Demand Response in Electricity Markets and Recommendations for
740 Achieving Them, (2006).
- 741 [6] A. Arteconi, N.J. Hewitt, F. Polonara, Domestic demand-side management (DSM): Role of heat pumps and
742 thermal energy storage (TES) systems, *Appl. Therm. Eng.* (2013).
743 <https://doi.org/10.1016/j.applthermaleng.2012.09.023>.
- 744 [7] W. Li, L. Yang, Y. Ji, P. Xu, Estimating demand response potential under coupled thermal inertia of
745 building and air-conditioning system, *Energy Build.* (2019). <https://doi.org/10.1016/j.enbuild.2018.10.022>.
- 746 [8] C. Yan, F. Wang, Y. Pan, K. Shan, R. Kosonen, A multi-timescale cold storage system within energy
747 flexible buildings for power balance management of smart grids, *Renew. Energy.* (2020).
748 <https://doi.org/10.1016/j.renene.2020.07.079>.
- 749 [9] A. Arteconi, J. Xu, E. Ciarrocchi, L. Paciello, G. Comodi, F. Polonara, R. Wang, Demand Side Management
750 of a Building Summer Cooling Load by Means of a Thermal Energy Storage, in: *Energy Procedia*, 2015.
751 <https://doi.org/10.1016/j.egypro.2015.07.705>.
- 752 [10] R. Tang, S. Wang, C. Yan, A direct load control strategy of centralized air-conditioning systems for building
753 fast demand response to urgent requests of smart grids, *Autom. Constr.* (2018).
754 <https://doi.org/10.1016/j.autcon.2017.12.012>.
- 755 [11] A. Malik, N. Haghdadadi, I. MacGill, J. Ravishankar, Appliance level data analysis of summer demand
756 reduction potential from residential air conditioner control, *Appl. Energy.* (2019).
757 <https://doi.org/10.1016/j.apenergy.2018.11.010>.
- 758 [12] N. Qi, L. Cheng, H. Xu, K. Wu, X.L. Li, Y. Wang, R. Liu, Smart meter data-driven evaluation of
759 operational demand response potential of residential air conditioning loads, *Appl. Energy.* (2020).
760 <https://doi.org/10.1016/j.apenergy.2020.115708>.
- 761 [13] S. Huang, D. Wu, Validation on aggregate flexibility from residential air conditioning systems for building-
762 to-grid integration, *Energy Build.* (2019). <https://doi.org/10.1016/j.enbuild.2019.07.043>.
- 763 [14] A. Arteconi, A. Mugnini, F. Polonara, Energy flexible buildings: A methodology for rating the flexibility
764 performance of buildings with electric heating and cooling systems, *Appl. Energy.* (2019).
765 <https://doi.org/10.1016/j.apenergy.2019.113387>.
- 766 [15] A. Mugnini, F. Polonara, A. Arteconi, Quantification of energy flexibility from air conditioning of
767 residential buildings, in: *Refrig. Sci. Technol.*, 2019. 10.18462/iir.icr.2019.966.
- 768 [16] S.J. Pedersen CO, Fisher DE, ASHRAE. Cooling and heating load calculation principles., 1998.
- 769 [17] A. Boodi, K. Beddiar, Y. Amirat, M. Benbouzid. Simplified Building Thermal Model Development and
770 Parameters Evaluation Using a Stochastic Approach, *Energies.* 13(11), 2899 (2020).
771 doi.org/10.3390/en13112899
- 772 [18] Un.E. ISO, EN ISO 13790. Energy performance of buildings Calculation of energy use for space heating
773 and cooling, (2008) 1–24.
- 774 [19] W.D. Dieter Patteeuw, Kenneth Bruninx, Alessia Arteconi, Erik Delarue, L. Helsen, Integrated modeling of
775 active demand response with electric heating systems coupled to thermal energy storage systems, *Appl.*
776 *Energy.* 151 (2015) 306–319. doi.org/10.1016/j.apenergy.2015.04.014.
- 777 [20] TRNSYS, TRNSYS 17 Documentation, Univ. Wisconsin-Madison. (2012).
- 778 [21] W. Cui, Y. Ding, H. Hui, M. Li, Two-stage payback model for the assessment of curtailment services
779 provided by air conditioners, in: *Energy Procedia*, 2017. doi.org/10.1016/j.egypro.2017.12.409.
- 780 [22] V. Corrado, I. Ballarini, S.P. Corgnati, Typology Approach for Building Stock: D6.2 National scientific
781 report on the TABULA activities in Italy, 2012.

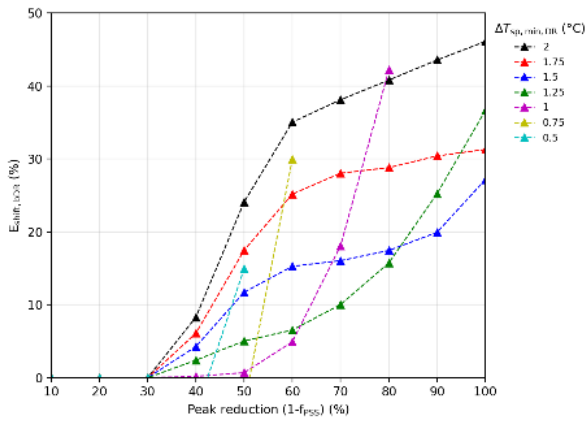
782 [23] UNI/TR 11552, Opaque envelope components of buildings Thermo-physical parameters, (2014) 1–44.
783 [24] Weather Data. energyplus.net/weather [accessed 7.04.2021].
784 [25] Viessmann, VITOCCELL 100-E/-W, Commer. Cat. [www.viessmann.it/it/riscaldamento-casa/bollitori-e-](http://www.viessmann.it/it/riscaldamento-casa/bollitori-e-serbatoi-per-acqua-calda/serbatoi-accumulo-acqua-di-riscaldamento/vitocell-100ew.html)
785 [serbatoi-per-acqua-calda/serbatoi-accumulo-acqua-di-riscaldamento/vitocell-100ew.html](http://www.viessmann.it/it/riscaldamento-casa/bollitori-e-serbatoi-per-acqua-calda/serbatoi-accumulo-acqua-di-riscaldamento/vitocell-100ew.html) [accessed
786 7.04.2021].
787 [26] Viessmann, VITOCAL 200-S, Commer. Cat. [www.viessmann.it/it/riscaldamento-casa/pompe-di-](http://www.viessmann.it/it/riscaldamento-casa/pompe-di-calore/pompe-di-calore-aria-acqua-split/vitocal-200-s.html)
788 [calore/pompe-di-calore-aria-acqua-split/vitocal-200-s.html](http://www.viessmann.it/it/riscaldamento-casa/pompe-di-calore/pompe-di-calore-aria-acqua-split/vitocal-200-s.html) [accessed 7.04.2021].
789 [27] R. Group, ECOdry CN+. Dehumidifier for radiant cooling., [www.rossatogroup.com/prodotti/trattamento-](http://www.rossatogroup.com/prodotti/trattamento-aria/deumidificatori-radiante/deumidificatore-radiante-controsoffitto.html)
790 [aria/deumidificatori-radiante/deumidificatore-radiante-controsoffitto.html](http://www.rossatogroup.com/prodotti/trattamento-aria/deumidificatori-radiante/deumidificatore-radiante-controsoffitto.html) [accessed 7.04.2021].
791
792
793
794
795
796
797
798
799
800
801
802
803
804
805
806
807
808
809
810
811
812
813
814
815
816
817
818
819
820
821
822
823
824
825
826
827
828
829
830

831 **APPENDIX A:**
 832 **Fan coil units (FCUs) with variable capacity heat pump (no TES configuration)**
 833

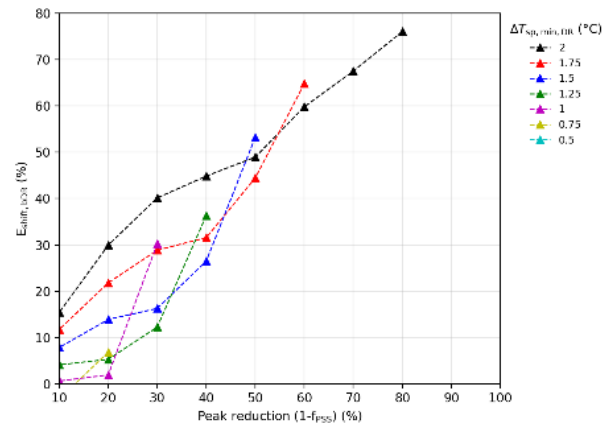


834 **Figure A1.** Flexibility curve: pre-cooling of the internal air node duration (Δk_{prec}) for FCU without TES for different peak
 835 reductions (f_{PSS}): (a) $\Delta T_{sp,min,DR}$ equal to 1 °C and variable $\Delta T_{sp,max,DR}$, (b) $\Delta T_{sp,min,DR}$ equal to 2 °C and variable $\Delta T_{sp,max,DR}$, (c)
 836 $\Delta T_{sp,max,DR}$ equal to 0.5 °C and variable $\Delta T_{sp,min,DR}$ and (d) $\Delta T_{sp,max,DR}$ equal to 0 °C and variable $\Delta T_{sp,min,DR}$.
 837





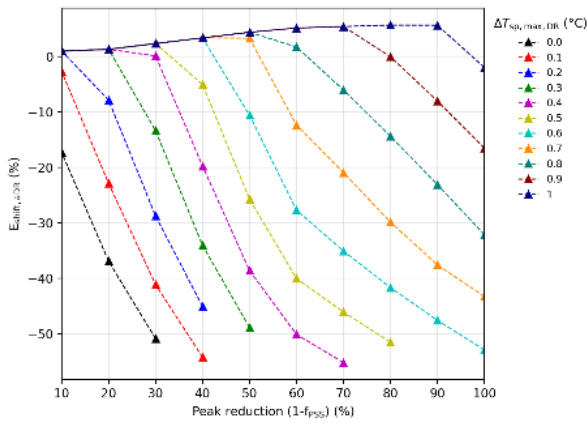
(c)



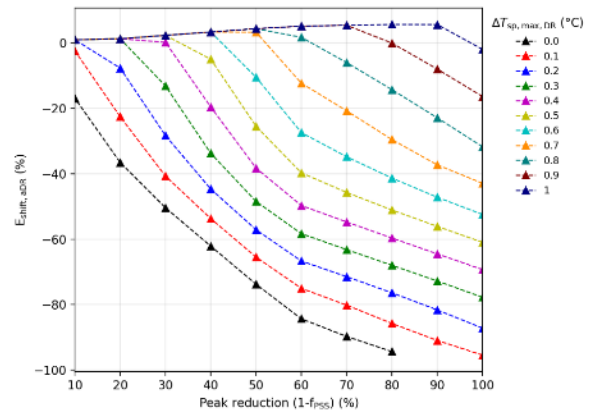
(d)

838 **Figure A2.** Flexibility curve: $E_{\text{shift,bDR}}$ for FCU without TES for different peak reductions (f_{PSS}): (a) $\Delta T_{\text{sp,min,DR}}$ equal to 1 °C and
 839 variable $\Delta T_{\text{sp,max,DR}}$, (b) $\Delta T_{\text{sp,min,DR}}$ equal to 2 °C and variable $\Delta T_{\text{sp,max,DR}}$, (c) $\Delta T_{\text{sp,max,DR}}$ equal to 0.5 °C and variable $\Delta T_{\text{sp,min,DR}}$ and
 840 (d) $\Delta T_{\text{sp,max,DR}}$ equal to 0 °C and variable $\Delta T_{\text{sp,min,DR}}$.

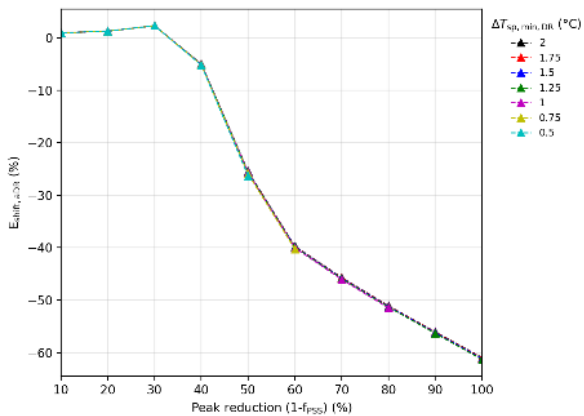
841



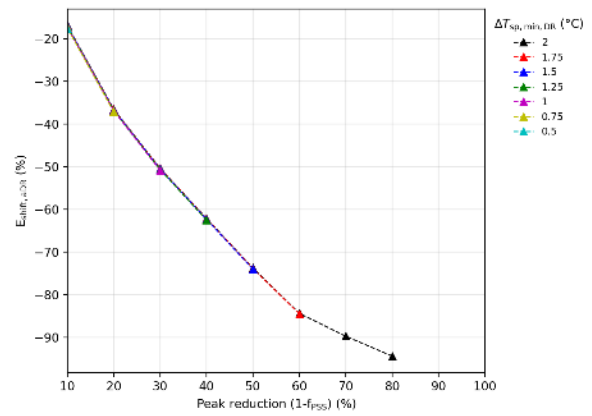
(a)



(b)



(c)



(d)

842 **Figure A3.** Flexibility curve: $E_{\text{shift,aDR}}$ for FCU without TES for different peak reductions (f_{PSS}): (a) $\Delta T_{\text{sp,min,DR}}$ equal to 1 °C and
 843 variable $\Delta T_{\text{sp,max,DR}}$, (b) $\Delta T_{\text{sp,min,DR}}$ equal to 2 °C and variable $\Delta T_{\text{sp,max,DR}}$, (c) $\Delta T_{\text{sp,max,DR}}$ equal to 0.5 °C and variable $\Delta T_{\text{sp,min,DR}}$ and
 844 (d) $\Delta T_{\text{sp,max,DR}}$ equal to 0 °C and variable $\Delta T_{\text{sp,min,DR}}$.

845

846

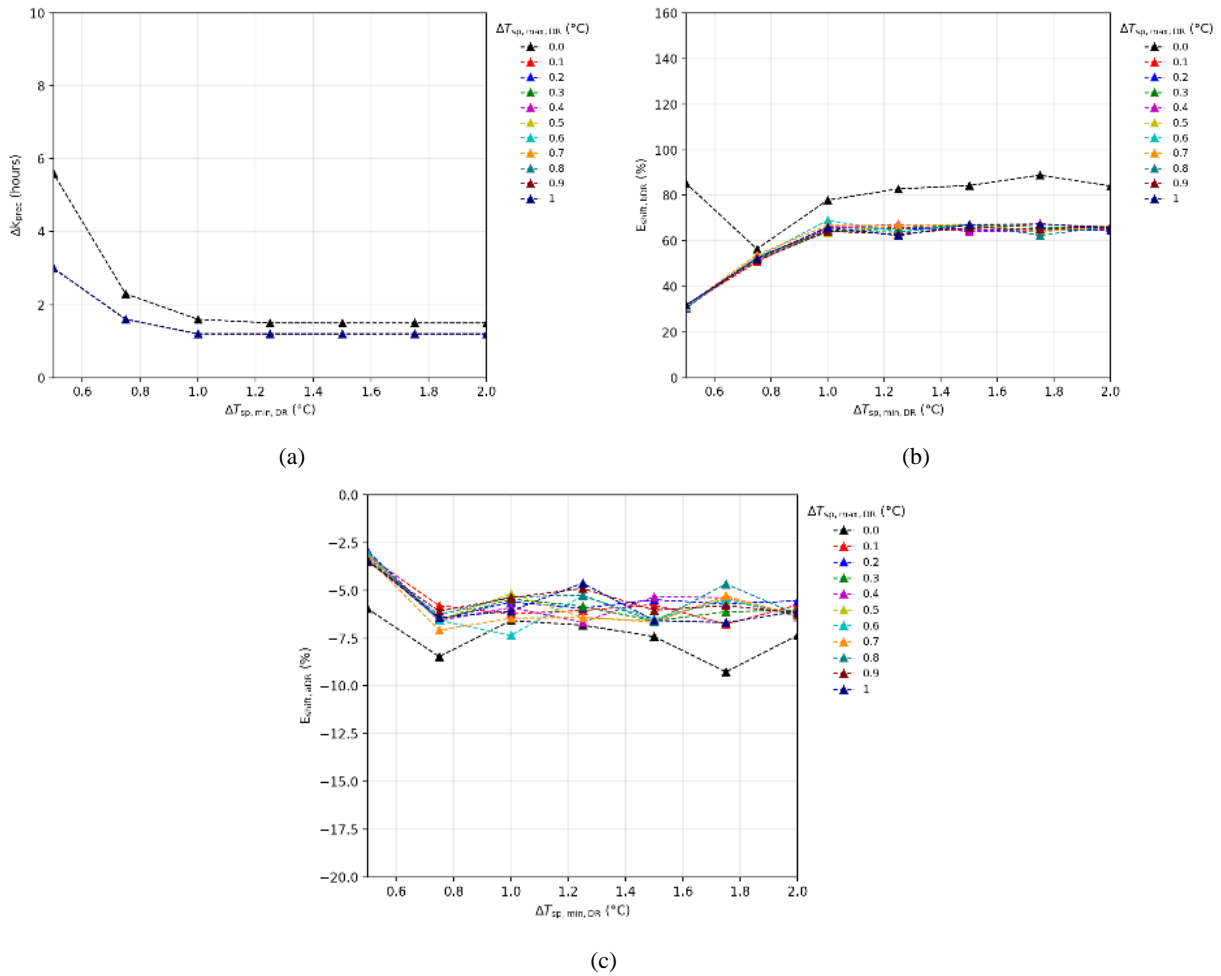
847

848

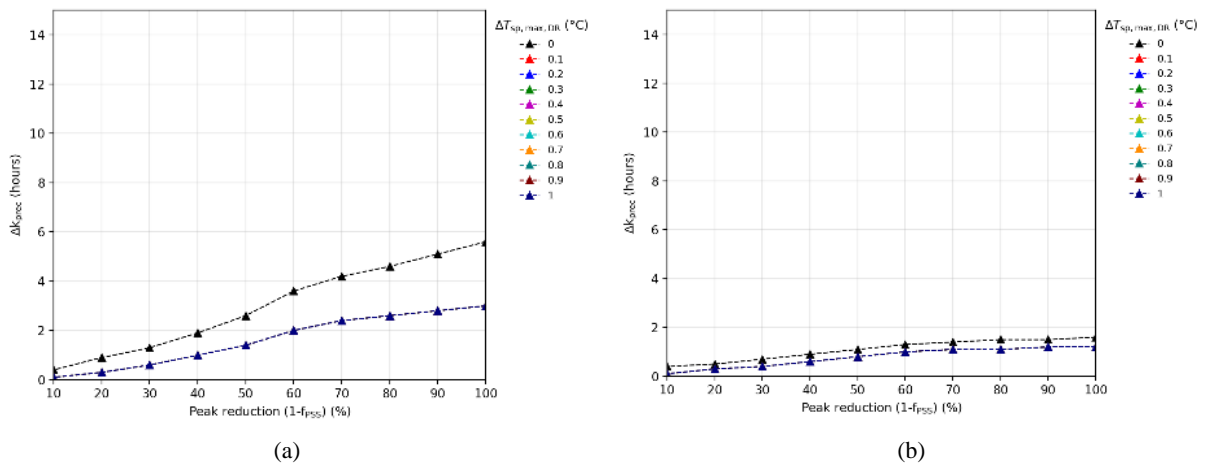
849

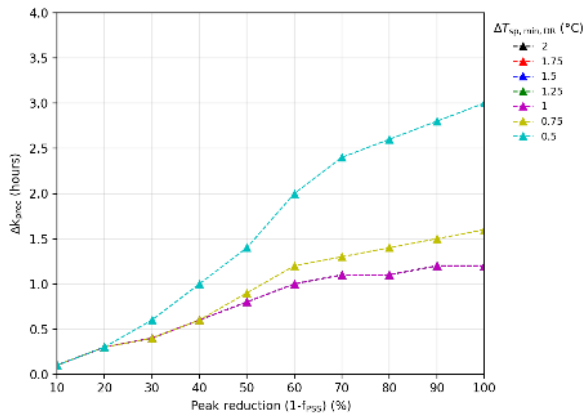
850

851 **APPENDIX B:**
 852 **Cooling ceiling panels (CP) with dehumidifier (DH)**
 853

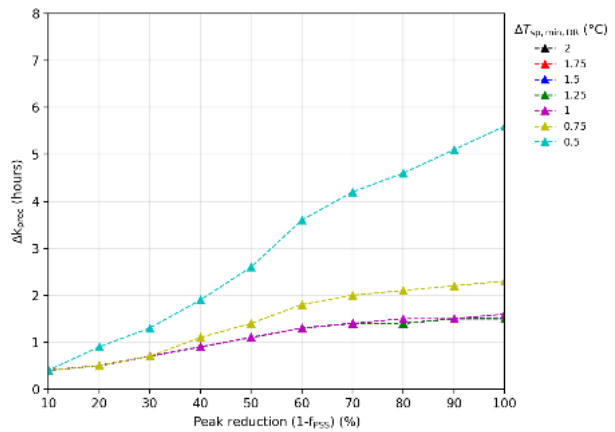


854 **Figure B1.** Daily flexibility curves for an event with f_{PSS} equal to 0 (100% peak reduction) and Δk_{DR} of 1 hour as the $\Delta T_{sp,max,DR}$
 855 and $\Delta T_{sp,min,DR}$ vary for CP ($\Delta RH_{sp,max,DR}$ and $\Delta RH_{sp,min,DR}$ equal to 10 %): (a) Pre-cooling of the internal air node duration (Δk_{prec}),
 856 (b) $E_{shift,bDR}$ and (c) $E_{shift,aDR}$





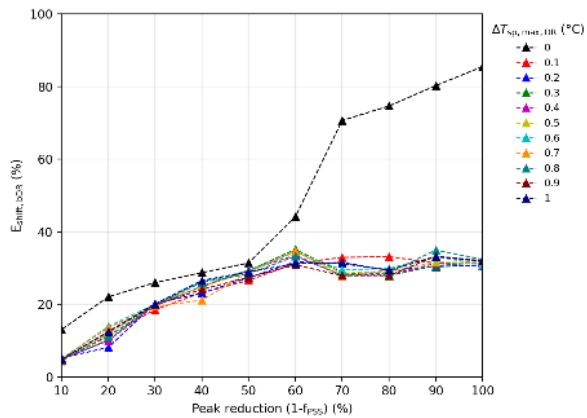
(c)



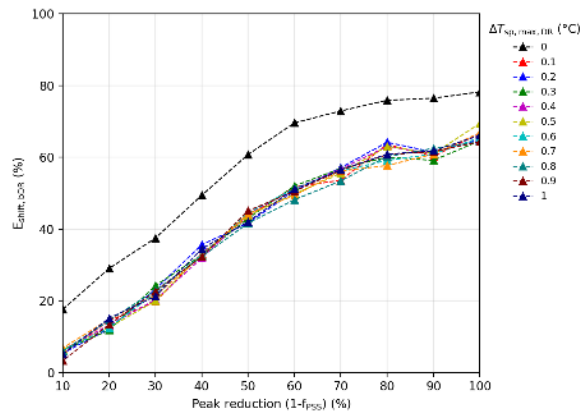
(d)

857 **Figure B2.** Flexibility curve: Pre-cooling of the internal air node duration (Δk_{prec}) for CP for different peak reductions (f_{PSS}): (a)
 858 $\Delta T_{\text{sp,min,DR}}$ equal to 0.5 °C and variable $\Delta T_{\text{sp,max,DR}}$, (b) $\Delta T_{\text{sp,min,DR}}$ equal to 1 °C and variable $\Delta T_{\text{sp,max,DR}}$, (c) $\Delta T_{\text{sp,max,DR}}$ equal to 0.5
 859 °C and variable $\Delta T_{\text{sp,min,DR}}$ and (d) $\Delta T_{\text{sp,max,DR}}$ equal to 0 °C and variable $\Delta T_{\text{sp,min,DR}}$. All the figures are realized with $\Delta RH_{\text{sp,max,DR}}$
 860 equal to 5 %.

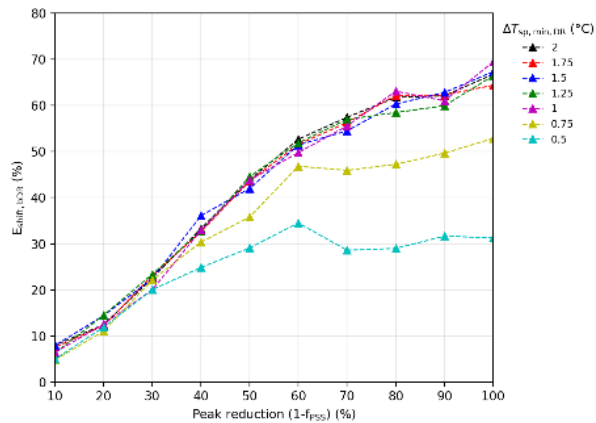
861



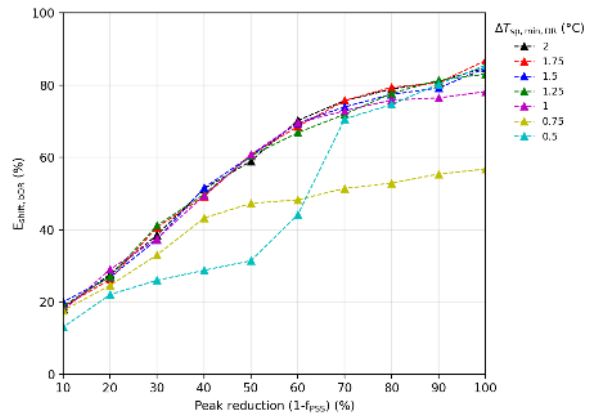
(a)



(b)



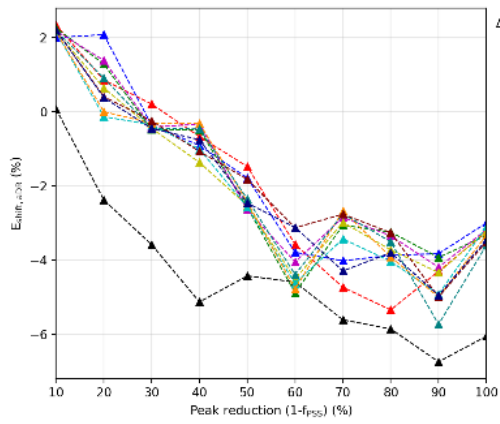
(c)



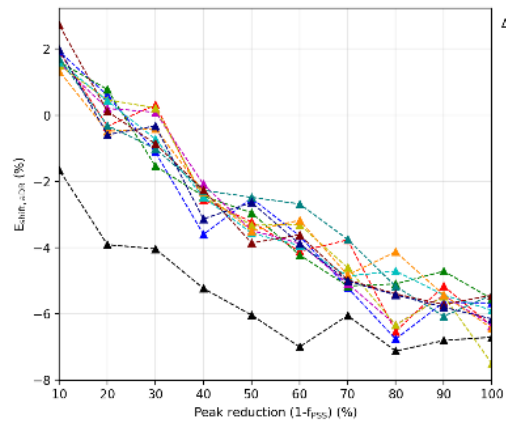
(d)

862 **Figure B3.** Flexibility curve: $E_{\text{shift,bDR}}$ for CP for different peak reductions (f_{PSS}): (a) $\Delta T_{\text{sp,min,DR}}$ equal to 0.5 °C and variable
 863 $\Delta T_{\text{sp,max,DR}}$, (b) $\Delta T_{\text{sp,min,DR}}$ equal to 1 °C and variable $\Delta T_{\text{sp,max,DR}}$, (c) $\Delta T_{\text{sp,max,DR}}$ equal to 0.5 °C and variable $\Delta T_{\text{sp,min,DR}}$ and (d)
 864 $\Delta T_{\text{sp,max,DR}}$ equal to 0 °C and variable $\Delta T_{\text{sp,min,DR}}$. All the figures are realized with $\Delta RH_{\text{sp,max,DR}}$ equal to 5 %.

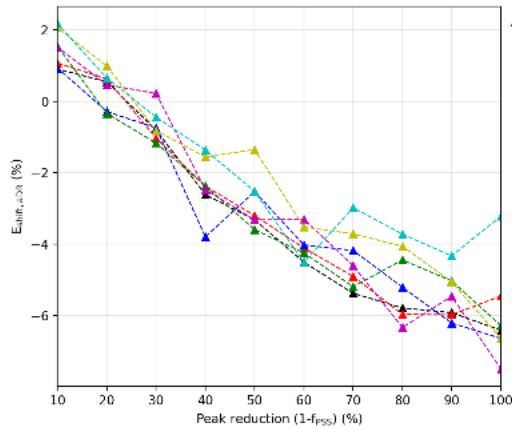
865



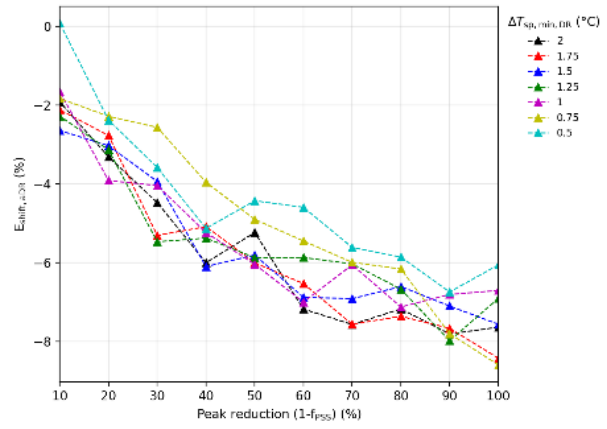
(a)



(b)



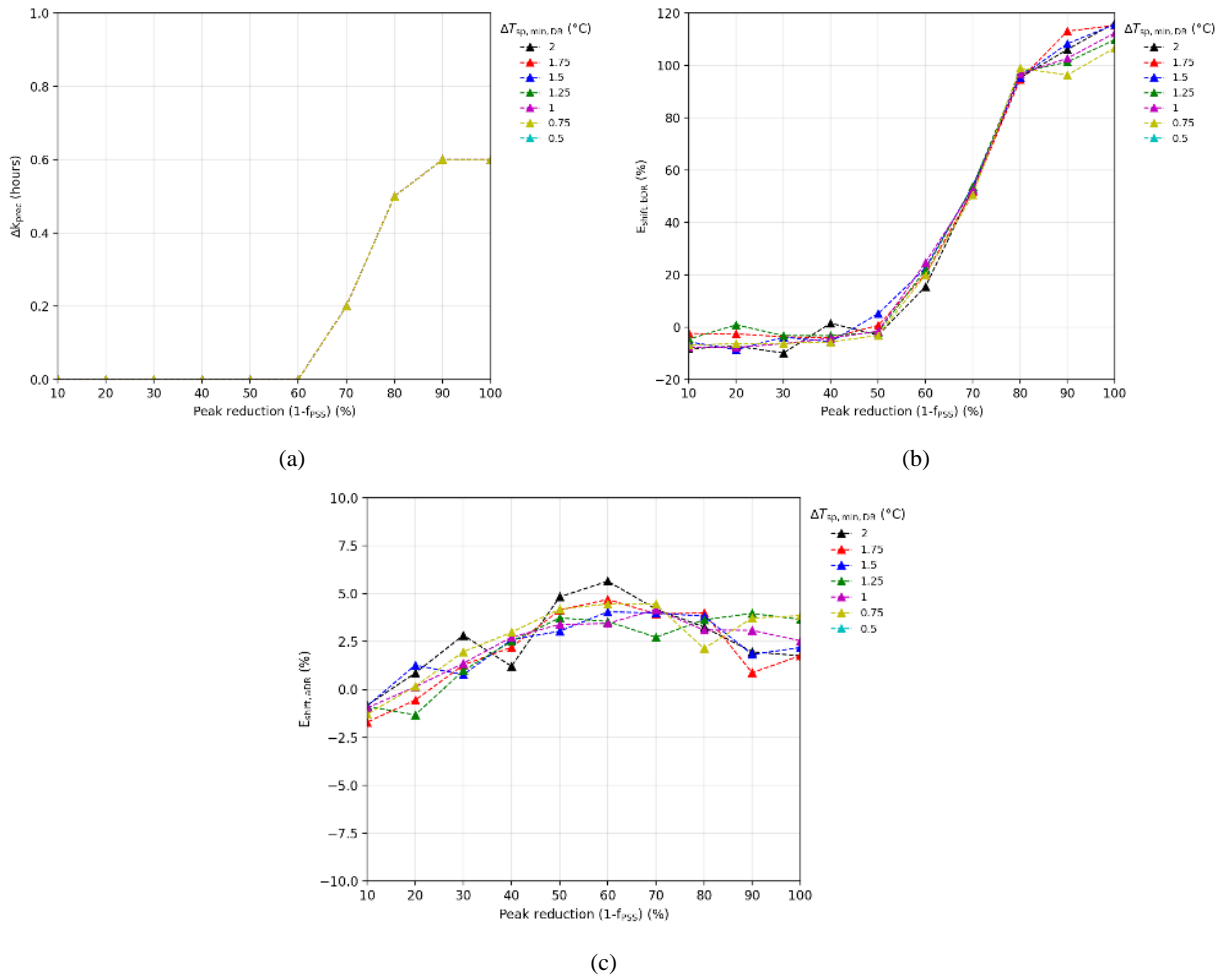
(c)



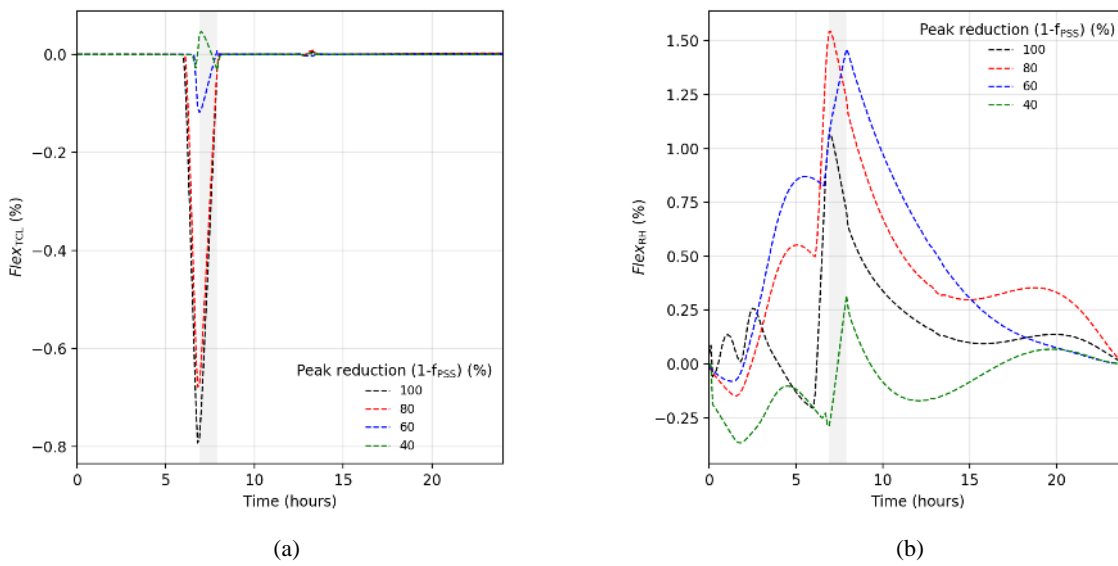
(d)

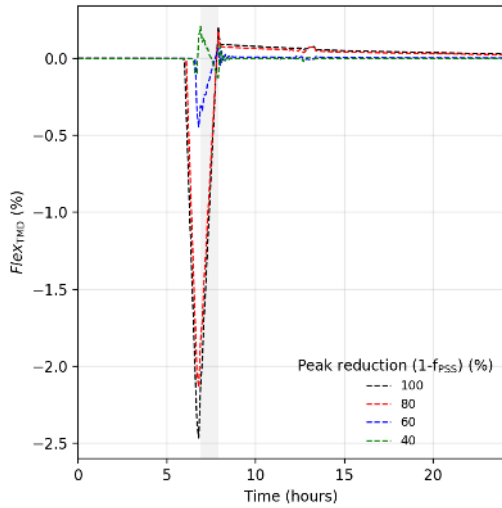
866 **Figure B4.** Flexibility curve: $E_{\text{shift,aDR}}$ for CP for different peak reductions (f_{PSS}): (a) $\Delta T_{\text{sp,min,DR}}$ equal to 0.5 °C and variable
 867 $\Delta T_{\text{sp,max,DR}}$, (b) $\Delta T_{\text{sp,min,DR}}$ equal to 1 °C and variable $\Delta T_{\text{sp,max,DR}}$, (c) $\Delta T_{\text{sp,max,DR}}$ equal to 0.5 °C and variable $\Delta T_{\text{sp,min,DR}}$ and (d)
 868 $\Delta T_{\text{sp,max,DR}}$ equal to 0 °C and variable $\Delta T_{\text{sp,min,DR}}$. All the figures are realized with $\Delta RH_{\text{sp,max,DR}}$ equal to 5 %.

869

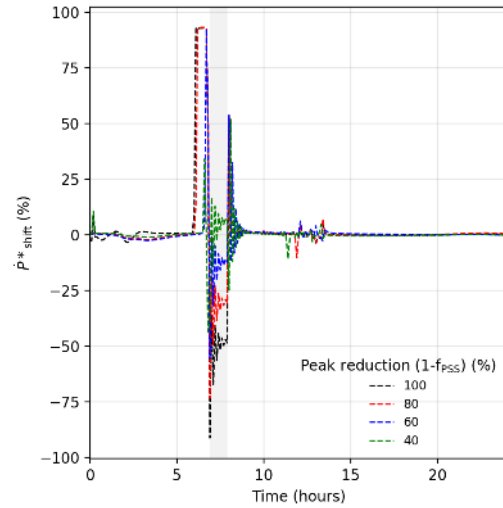


872 **Figure C1.** Daily flexibility curves for an event with $\Delta T_{sp,max,DR}$ equal to 1 °C and Δk_{DR} of 1 hour as the $\Delta T_{sp,min,DR}$ and the peak
 873 reduction (f_{PSS}) vary for CC ($\Delta RH_{sp,max,DR}$ and $\Delta RH_{sp,min,DR}$ equal to 5 %): (a) Pre-cooling of the internal air node duration (Δk_{prec}),
 874 (b) $E_{shift,bDR}$ and (c) $E_{shift,aDR}$.
 875



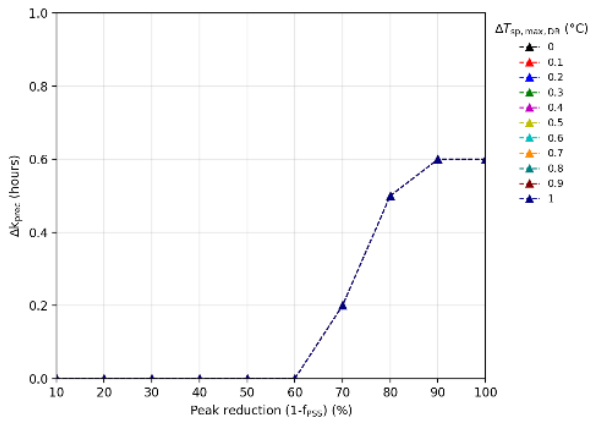


(c)

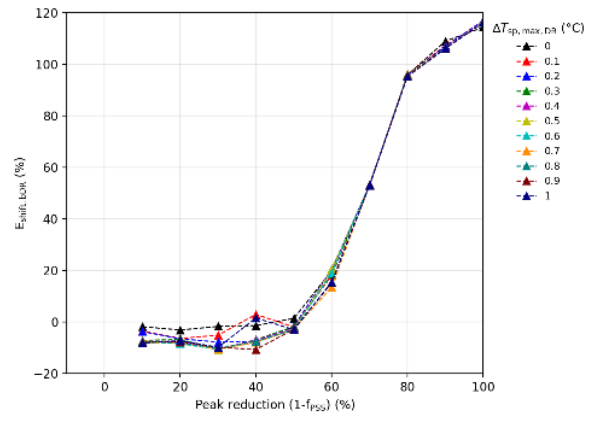


(d)

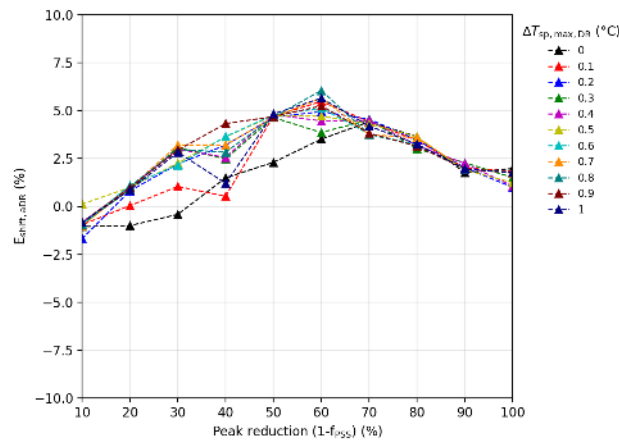
876 **Figure C2.** Daily demand response operation (f_{PSS} of 0, 0.2, 0.4 and 0.6, Δk_{DR} of 1 hour, $\Delta T_{sp,max,DR}$ of 1 °C and $\Delta T_{sp,min,DR}$ of 2 °C)
 877 for CC ($\Delta RH_{sp,max,DR}$ and $\Delta RH_{sp,min,DR}$ equal to 5 %): (a) $Flex_{TCL}$, (b) $Flex_{RH}$, (c) $Flex_{TMD}$ and (d) \dot{P}^*_{shift} .
 878



(a)



(b)



(c)

879 **Figure C3.** Daily flexibility curves for an event with $\Delta T_{sp,min,DR}$ equal to 2 °C and Δk_{DR} of 1 hour as the $\Delta T_{sp,max,DR}$ and the peak
 880 reduction (f_{PSS}) vary for CC ($\Delta RH_{sp,max,DR}$ and $\Delta RH_{sp,min,DR}$ equal to 5 %): (a) Pre-cooling of the internal air node duration (Δk_{prec}),
 881 (b) $E_{shift,bDR}$ and (c) $E_{shift,aDR}$.
 882